This is a preprint, the final version is subject to change, of the American Mineralogist (MSA)
Cite as Authors (Year) Title. American Mineralogist, in press.
DOI: https://doi.org/10.2138/am-2019-7068

Revision 2

Crystallographic and fluid compositional effects on the halogen (Cl, F, Br, I) incorporation in pyromorphite-group minerals

Tatjana Epp[1,5*], Michael A.W. Marks,[1], Thomas Ludwig[2], Mark A. Kendrick[3], Nelson Eby[4], Harald Neidhardt[5], Yvonne Oelmann[5], Gregor Markl[1]

[1] Eberhard Karls Universität Tübingen, Fachbereich Geowissenschaften, Wilhelmstraße 56, 72076 Tübingen, Germany, +49(0)70712973165 tatjanaepp@web.de, michael.marks@uni-tuebingen.de, gregor.markl@uni-tuebingen.de

[2] Ruprecht-Karls-Universität Heidelberg, Institut für Geowissenschaften, Im Neuenheimer Feld 234-236, 69120 Heidelberg, Germany, thomas.ludwig@geow.uni-heidelberg.de

[3] Research School of Earth Sciences, Australian National University, 142 Mills Rd, Acton, ACT, 0200, Australia, mark.kendrick@anu.edu.au

[4] Department of Environmental, Earth and Atmospheric Sciences, University of Massachusetts, Lowell, MA, 01854, USA, G_Eby@uml.edu

[5] Eberhard Karls Universität Tübingen, Fachbereich Geoökologie, Rümelinstraße 19-23, 72070 Tübingen, Germany, yvonne.oelmann@uni-tuebingen.de, harald.neidhardt@uni-tuebingen.de

*Corresponding author: Tatjana Epp, tatjanaepp@web.de

This is a preprint, the final version is subject to change, of the American Mineralogist (MSA)
Cite as Authors (Year) Title. American Mineralogist, in press.
DOI: https://doi.org/10.2138/am-2019-7068

1. Abstract

Pyromorphite-group minerals (PyGM), mainly pyromorphite ($Pb_5(PO_4)_3Cl$), mimetite ($Pb_5(AsO_4)_3Cl$) and vanadinite ($Pb_5(VO_4)_3Cl$), are common phases that form by supergene weathering of galena. Their formation is strongly influenced by processes at the Earth's surface and in the soil overlying a lead deposit and they incorporate high amounts of halogens, mostly Cl and, in some cases, F. The abundance of Br and I in natural PyGM and their potential as process tracers during surface and sub-surface fluid-rock interaction processes has not been investigated in detail due to analytical difficulties. We therefore developed methods for the simultaneous determination of Cl, F, Br and I in PyGM for (1) powdered bulk samples via Combustion Ion Chromatography (CIC) and (2) compositionally zoned crystals by means of Secondary Ion Mass spectrometry (SIMS).

Our study is based on well-characterized samples of pyromorphite (N=38), mimetite (N=16) and vanadinite (N=2) from Schwarzwald (Germany). Natural pyromorphite incorporates more I (up to 26 $\mu g\ g^{-1}$) than mimetite (up to 2 $\mu g\ g^{-1}$) and vanadinite (up to 1 $\mu g\ g^{-1}$), while Br contents are higher in mimetite (up to 20 $\mu g\ g^{-1}$) and vanadinite (up to 13 $\mu g\ g^{-1}$) compared to pyromorphite (less than 4 $\mu g\ g^{-1}$). These results are unexpected, as mimetite and vanadinite have longer As/V-O bonds giving them larger unit cells and larger polyhedral volumes for the Cl site in the $Pb2_6$ octahedron than pyromorphite. Accordingly, pyromorphite was expected to preferentially incorporate Br rather than I but the opposite is observed. Hence, halogen chemistry of PyGM is probably not governed by a crystal-chemical control (alone) but by fluid composition. However, the exact reasons remain enigmatic. This idea is corroborated by spatially resolved SIMS analyses which show that many pyromorphite-group minerals are strongly zoned with respect to their halogen mass ratios (e.g., Br/Cl, Br/I mass ratios). Furthermore, variations in halogen abundance ratios do not correlate with Ca/Pb, P/As or P/V ratios and therefore may record alternating and season-dependent environmental parameters

48 including biological activity, vegetation density, physico-chemical soil properties and rainfall
49 rate. We suggest that the zonation reflects multiple single fluid flow episodes and, hence,
50 records surface processes. However, further experiments concerning the fractionation of
51 halogens between fluid and PyGM are needed before halogen ratios in pyromorphite-group
52 minerals can be used as reliable monitors of fluid-driven processes.

53

54 **Keywords:** bromine, iodine, combustion ion chromatography, pyromorphite, mimetite,
55 vanadinite

56

57 ## 2. Introduction

58 More than 1500 localities (www.mindat.org) are known to contain pyromorphite-group
59 minerals (PyGM). The supergene weathering of ore deposits plays a major role in both
60 mobilizing and re-precipitating toxic trace elements such as Pb, As, Cd and Sb (Reich and
61 Vasconcelos, 2015; Siegel, 2002). Dissolution of primary minerals and precipitation of
62 secondary mineral phases during oxidation is mainly governed by fluid flow from the surface
63 through soil and fractured rocks into and through ore deposits (Basta and McGowen, 2004;
64 Ruby et al., 1994). The most abundant Pb-bearing ore mineral is galena (PbS). During
65 supergene weathering of galena, pyromorphite-group minerals (PyGM) form in the immediate
66 environment (e.g., Keim and Markl, 2015; Park Jr and MacDiarmid, 1975; Ruby et al., 1994).
67 Due to their extremely low solubility products (logK values in the range of -75 to -86; Bajda,
68 2010; Flis et al., 2007; Gerke et al., 2009; Nriagu, 1973), Pb, As, V and other toxic metals
69 (e.g., Cr, Sb, Bi, U) are immobilized and their bioavailability is thereby reduced when PyGM
70 form (e.g., Burmann et al., 2013; Flis et al., 2011; Markl et al., 2014).

As part of the apatite supergroup, the generalized formula for PyGM is Pb_5A_3L, where A represents PO_4^{3-} (pyromorphite), AsO_4^{3-} (mimetite) or VO_4^{3-} (vanadinite) and L is mostly comprised of Cl^-, F^-, OH^-, Br^- and/or I^- (e.g., Knyazev et al., 2011; Markl et al., 2014; Wondratschek, 1963). Structurally related members of the hedyphane group (hedyphane, phosphohedyphane, and fluoro-phosphohedyphane) have the composition $Ca_2Pb_3A(Cl^-, OH^-, F^-)$, where A is either PO_4^{3-} or AsO_4^{3-} (Pasero et al., 2010). There exists complete miscibility between pyromorphite and mimetite, pyromorphite and phosphohedyphane, and between mimetite and hedyphane (e.g., Dennen, 1960; Flis et al., 2011; Förtsch and Wondratschek, 1965; Markl et al., 2014; Wondratschek, 1963). Based on the presently available data on natural samples, the miscibility gap between vanadinite and pyromorphite allows for up to 3 mol % vanadinite component in pyromorphite and up to 39 mol % pyromorphite component in vanadinite (Markl et al., 2014).

The halogen site in PyGM is mostly occupied by Cl^-, but can also incorporate significant F^- and OH^- (Markl et al., 2014). However, the only naturally occurring F-dominated endmember is phosphohedyphane (Kampf and Housley, 2011; Pasero et al., 2010). Markl et al. (2014) identified the occurrence of naturally existing hydroxylmimetite, in which the crystallographic site is dominantly occupied by an OH-endmember. A further natural OH-endmember hydroxylpyromorphite was described (Hålenius et al., 2017). Halogen (F, Cl, Br) endmembers have been synthesized (except for I-pyromorphite; Janicka et al., 2012; Wondratschek, 1963) and thus appear to be thermodynamically stable at near-surface conditions (Janicka et al., 2012; Wondratschek, 1963). However, little is known about the natural abundance of Br and I in these minerals due to their low concentrations in natural fluids (Fuge, 1988; Schnetger and Muramatsu, 1996) and a lack of suitable analytical techniques.

The variation of halogen contents and halogen ratios (e.g., Br/Cl, F/Cl, Br/I) in a range of minerals including apatite, mica, amphibole, serpentine and scapolite are used to decipher

fluid-involving processes, such as magmatic degassing, metasomatism or hydrothermal processes during fluid-rock interaction and ore formation (e.g., Boyce and Hervig, 2009; Burisch et al., 2016; Harlov, 2015; Harlov et al., 2005; John et al., 2011; Kendrick and Phillips, 2009; Kendrick et al., 2013; Kendrick et al., 2015; Kusebauch et al., 2015a; Marks et al., 2012; Teiber et al., 2015; Walter et al., 2018; Webster and Piccoli, 2015). For apatite in particular, it was shown that crystal and fluid chemical processes control halogen incorporation (Kusebauch et al., 2015a). Due to structural similarities between apatite and PyGM, we suggest that halogen contents and ratios in PyGM may also serve as recorders of fluid processes in the near-surface environments. Based on geochemical considerations and estimations of the growth rate of PyGM, compositional zonation in PyGM may even reflect seasonal changes in precipitation and/or changes in the intensity of host rock alteration. This potentially monitors the variable importance of diverse fluid sources and of processes changing the fluids' composition during their growth (Keim and Markl, 2015; Markl et al., 2014).

As a first step towards testing the capability of PyGM for monitoring such processes, we present halogen (Cl, F, Br, I) data for a comprehensive set of PyGM from the Schwarzwald mining district in SW Germany. We developed a method for determining bulk halogen contents in PyGM via Combustion Ion Chromatography (CIC), which was cross-calibrated with data from Instrumental Neutron Activity Analysis (INAA) and a noble gas technique (NG; Kendrick, 2012, 2018). Further, Secondary Ion Mass Spectrometry (SIMS) were used to resolve small-scale halogen variations in single PyGM crystals.

3. Material and methods

3.1. Samples and geological background

The samples for this study originate from the Schwarzwald, SW Germany (Fig. 1), a part of the Central European Variscan fold belt composed of crystalline basement rocks (mainly gneisses and granites), which are overlain by a sequence of terrestrial and marine sedimentary cover rocks (Timmerman and McCann, 2008). The Schwarzwald hosts more than 1,000 hydrothermal veins (Metz and Richter, 1957) with a large variety of mineral assemblages, which have formed continuously between about 310 Ma and today (e.g., Pfaff et al., 2009; Staude et al., 2009; Walter et al., 2016). The hydrothermal veins most important for the present study consist of galena-sphalerite(±chalcopyrite)-bearing assemblages, which are commonly embedded in barite, fluorite, calcite or quartz.

The PyGM samples investigated in this study are from the entire Schwarzwald region, with many samples from the Kinzigtal area (central Schwarzwald), the Münstertal-Schauinsland-Todtnau region and the area around St. Blasien (southern Schwarzwald). The samples are from 23 different sites (Fig. 1, Tab. 1), where the hydrothermal veins are hosted either by basement granites, schists, rhyolites, gneisses and migmatites or quartzitic sandstones of the sedimentary cover. The samples for this study represent a carefully selected subset of the samples that were previously analyzed by Markl et al. (2014) for their major and trace element composition. They comprise a large variety of colors (green, brown, orange and yellow) and textures (euhedral, prismatic crystals, microcrystalline needles, spherical aggregates, as well as crusts and sinters) and cover a broad range of geological, regional and compositional variation (Tab.1). Based on previous data (Markl et al., 2014), most samples either show P # (= P/P+As+V) <0.2 (= mimetite, vanadinite) or >0.8 (= pyromorphite), with only few samples representing intermediate mineral compositions (Fig. 2).

The current oxidative weathering profile of these ore deposits began to develop at 12 Ma and is dominated by supergene minerals younger than 3 Ma (e.g., Hautmann and Lippolt, 2000; Hofmann and Eikenberg, 1991; Pfaff et al., 2009). The higher areas in the Schwarzwald

(including the Feldberg area) were extensively eroded during the last glacial period (Brook et al., 2000; Ehlers and Gibbard, 2004; Morel et al., 2003). Therefore, we assume that PyGM from areas that are today >900 m above sea level (localities 10-12, 15; Fig. 1; Tab. 1) were probably formed in the last 20,000 years. Some samples are demonstrably younger than 200 years because they occur as sinters on historic mine walls (localitites 4, 6-7, 12-13, 20-21; Fig. 1, Tab. 1).

3.2. Analytical Methods

In total, 41 samples from 23 sites were analyzed with CIC (2 vanadinites, 28 pyromorphites including 1 Pb-phosphohedyphane, and 11 mimetites including 1 mimetite with fluoro-phosphohedyphane zones; Tab. 1). A subset of 15 of these samples was analyzed by SIMS (10 pyromorphites including 1 Pb-phosphohedyphane and 5 mimetites including 1 mimetite with fluoro-phosphohedyphane zones).

3.2.1. Combustion Ion Chromatography (CIC). Combustion Ion Chromatography is an automated combination of combustion digestion (pyrohydrolysis) and ion chromatography. This method was used for the simultaneous determination of halogens (Cl, F, Br, I) at the Universität Tübingen. A 930 Compact IC Flex chromatograph (Metrohm) with chemical suppression and a peristaltic pump for regeneration (100 mmol/l H_2SO_4) connected to a combustion oven and an autosampler for solid samples (MMS 5000; Analytik Jena) was used.

For combustion, a mixture of equal amounts (9.9 – 10.5 mg) of powdered sample and WO_3 (99.995% - Aldrich 204781) was inserted into a quartz vial that was capped on both sides with quartz wool and placed into a glass vessel. The quartz vials were heated in an extraction line coupled to the IC with a constant flow of Ar (6.0; 100 ml/min) and O_2 (5.0; 300 ml/min) to 1050°C for 12 min, followed by 10 min of post-combustion and 7 min of cooling. During combustion, a constant water flow (0.2 ml/min) was maintained. The loaded steam was collected in an absorber module containing 10 ml of 500 µg/g H_2O_2 solution. After matrix

elimination (using a Metrosep A PCC 2 HC/4.0 column) the solutions were injected into the ion chromatograph. For improved detection of Br and I in the presence of high amounts of Cl, a Metrosep A Supp 5-250/4.0 (kept at 55°C) and a Metrosep A Supp 4/5/4.0 guard column and an eluent consisting of a mixture of 2 mmol NaOH (suprapure), 1.6 mmol Na_2CO_3 (suprapure), and 5 vol.% acetone at a flow rate of 0.7 ml/min was used. This eluent composition was chosen as it minimized the overlap between the Br and Cl signals and optimized the simultaneous detection of low Br concentrations (µg g^{-1}-level) in the presence of high Cl contents (wt%-level). However, a complete separation of the Br and Cl peaks was impossible to achieve and Br was quantified as a shoulder peak on the Cl signal. For the whole analytical procedure, Millipore water (18.2 MΩ*cm) was used.

For the calibration a primary reference solution was prepared by mixing single element-solutions of Cl, F, Br and I (Roth; 1000 mg l^{-1}) and a quadratic 6-point-calibration curve that covered the concentrations investigated was constructed using the Metrohm intelligent Partial Loop Injection Technique (MiPT). Quantification was done using MagIC Net software (Metrohm).

The effective detection limits for powdered samples were about 10-30 µg g^{-1} for F and Cl, about 0.1 µg g^{-1} for I, and around 0.3 µg g^{-1} for Br. Based on the frequent analyses of standard solutions and various reference materials (Tab.2), relative uncertainties were generally <10% (1-sigma level) for F and Cl, and up to ~ 20% for Br and I, depending on the concentrations.

3.2.2. Instrumental Neutron Activity Analysis (INAA). For cross-calibration with the CIC technique, sample PY-1 was analyzed for Br at University of Massachusetts, Lowell, using Instrumental Neutron Activation Analysis (INAA). Approximately 200 mg of sample was weighed into an acid-cleaned high-purity polyethylene vial. The sample was irradiated in-core for one hour and the nominal neutron flux was 10^{13} n $cm^{-2}s^{-1}$. Following a 5 to 7-day decay

period, the sample was counted for 10,000 s. The 554 and 777 keV gamma-ray energies (Br-82, half-life 35.3 h) were used for the analytical determinations. The 619 keV gamma-ray was not used because of potential interference from the 618.3 keV W-187 gamma-ray. Peak areas were determined using Canberra Genie software. Further data reduction for decay time, flux, and geometry was done using software developed in-house. The Br concentration was determined by reference to the NIST traceable Dionex Combined Seven Anion Standard II (Thermo Scientific).

3.2.3. Noble Gas (NG). For three samples (JH-053, JH-128 and PY-1), Cl, Br and I contents were determined from 5-30 mg size sample duplicates by the noble gas method (NG), which enables halogen measurement from irradiation-produced noble gas proxy isotopes (^{39}ArK, ^{38}ArCl, ^{80}KrBr, ^{128}XeI) (e.g., Johnson et al., 2000; Kendrick, 2012). The samples were irradiated for 50 hours in the Central Facility of the research reactor at the McClellan Nuclear Radiation Center, University of California, Davis, USA, on the 23rd August 2014 (Irradiation RS#1). The irradiation was monitored with Hb3Gr (1072 Ma; Roddick, 1983) and aliquots of 3 scapolite gems used as halogen standards (Kendrick, 2012; Kendrick et al., 2013). The samples received a total neutron fluence of 3.7×10^{18} n cm^{-2} with a fast/thermal ratio of 1 (J = 0.0096). Noble gases were extracted from the samples by fusion at 1500 °C in a tantalum resistance furnace and purified over 40 minutes on a series of Zr-Al getter pumps, which removes active gases such as H_2O, CO_2 and N_2. The purified noble gases were expanded into the MAP-215-50 noble gas mass spectrometer and sequentially analyzed for isotopes of Ar, Kr and Xe in peak jumping mode over a period of 45 minutes. This technique enables determination of Br/Cl and I/Cl ratios with analytical precision of 1-2% in a single irradiation. Scapolite standards calibrated relative to experimentally determined neutron capture cross sections have long term reproducibility of ~3-5% (1 s.d.) (Kendrick et al., 2013). However, Cl, Br and I concentrations are subject to an additional uncertainty related to mass

spectrometer sensitivity, giving a total uncertainty (accuracy) of c. ± 10% relative in concentrations (Kendrick et al., 2018).

3.2.4. Electron Probe Microanalysis. The composition of the samples analyzed by SIMS (section 3.2.5 and 4.5) was determined using a JEOL Superprobe JXA-8900RL at the Fachbereich Geowissenschaften, Universität Tübingen, Germany following the method described in Markl et al. (2014). Acceleration voltage of the defocused beam (15µm diameter) was 20 kV at a beam current of 20 nA. Counting times for major elements were 16 s for the element peak and 8 s for each background and for minor elements 30 s and 15 s, respectively. The following synthetic and natural standards were used for calibration: $Ca_5(PO_4)_3(F,Cl)$ for F(Kα) and Ca(Kα); $CaMgSi_2O_6$ for Si(Kα); UO_2 for U(Mα) and V for V(Kα). To improve the quality of the analyses, the external standards PY-1 $Pb_5(PO_4)_3Cl$ and MIM-1 $Pb_5(AsO_4)_3Cl$ were used for Pb, P, As and Cl (see details in Markl et al., 2014). An automatic φρz correction was applied to all analyses. Peak overlaps of Ca by Pb (Lγ 1, 4th order) and F by P (Kα 1 and 2, 3th order) were corrected internally. The detailed WDS configuration, including standards, counting times and the resulting average detection limits are given in the electronic supplement ESM 1.

3.2.5. Secondary Ion Mass Spectrometry (SIMS). SIMS analyses were performed using the Heidelberg Ion Probe (Cameca IMS 1280-HR) at the Institute of Earth Sciences, Heidelberg University. Cs^+ ions with a net energy of 23keV and a beam current of ~ 2 nA were focused to ~ 5 µm and rastered over an area of 10 µm x 10 µm. Negative secondary ions were accelerated to 10 keV with an offset of 50 V to the acceleration voltage. The normal incidence electron gun (NEG) was used to compensate for charge build-up on the samples, which were coated with ~ 50 nm of gold. The offset of 50 V was also applied to the acceleration voltage of the NEG. The width of the mass spectrometer's energy window was

set to 40 eV so that secondary ions with a starting energy of 70 ± 20 eV were transmitted (energy filtering to reduce the impact of molecular interferences). The mass resolving power was set to M/ΔM ≅ 2200. $^{35}Cl^-$ [20 s] was detected with the axial Faraday cup (R = $10^{11}\Omega$) while all other species (^{19}F [40 s], $^{40}Ca^{37}Cl$ [40 s], ^{81}Br [80 s] and ^{127}I [80 s] were detected with the axial electron multiplier in counting mode (the times given in square brackets are the total integration times). Prior to each analysis the sample was sputtered for 90 s with a raster size of 15 µm and the analysis started after a sputter time of ~ 190 s. There were two significant molecular interferences: $^{31}P^{16}O_2{}^{18}O$ and $^{44}Ca^{37}Cl$ on ^{81}Br. The first was fully resolved while the latter would have required a very high MRP (mass resolving power) of ~ 15900 and was not resolved. To correct for the contribution of $^{44}Ca^{37}Cl$ on the ^{81}Br peak the $^{40}Ca^{37}Cl$ intensity was extrapolated to $^{44}Ca^{37}Cl$ and subtracted (Marks et al., 2012). This resulted in relative corrections of 0 to –13 %.

The samples showed a strong increase of the halogen ion count rates during sputtering, as shown in Fig. 3a for sample PY-1. The increase of the count rates is very similar for all halogens, which results in reasonably constant ratios (Fig. 3b). For comparison, results using the same analytical setup are shown for an obsidian glass (Pichavant et al., 1987) in Figs. 3c and d. This glass (and other glasses) did not show this increase of halogen count rates. Because the count rates of all halogens increase simultaneously, Cl (major element in all samples investigated) was chosen as reference element. P was taken into consideration, but showed a completely different behavior over sputter time.

Halogen reference materials or standards for SIMS are in short supply (e.g., Kendrick et al., 2018; Marks et al., 2017) and is even worse for exotic minerals like PyGMs: there are no reference materials with a remotely similar matrix. For further detailed studies on such materials it is desirable to produce matrix-matched synthetic reference materials with known concentrations of the halogens. The ion yields (RIY) of F, Br and I relative to Cl were

therefore determined on samples JH-053, JH-128 and PY-1 using data from the other analytical methods. The results are presented in the electronic supplement 2. The mean value of the RIYs on these three reference samples was used to quantify the halogens in the unknown samples. It is currently not clear whether the high variation in the RIYs is caused by matrix effects, by the inhomogeneity of the reference samples, or other unknown factors. The accuracy of the SIMS data is therefore semi-quantitative at best. This should however not affect the data on relative halogen incorporation within one sample, which was the goal of the SIMS analyses.

4. Results

4.1. Consistency of the data set

Three samples (PY-1, JH-053 and JH-128) have been analyzed by EPMA (Markl et al., 2014 and this study), NG (this study) and INAA (only PY-1, this study) for testing the accuracy of the CIC method. The mean Cl concentrations based on CIC and EPMA data for PY-1, JH-053 and JH-128 show a maximum relative difference of 3 %, demonstrating the consistency between these two methods (Fig. 4; Tab. 2). For most samples investigated during this study, Cl contents determined by EPMA and CIC overlap within uncertainty (Fig. 4). Note that the relatively large range of EPMA data for some of the samples indicates strong compositional zonation, which is not mirrored in the CIC data, which derive from much larger bulk sample amounts. A few samples show higher EPMA than CIC-derived Cl concentrations (Fig. 4), which can, however, not be traced back to especially strong zonation in these samples. Accordingly, the reason for this observation remains unclear. The CIC determinations agreed within a 90% confidence interval with the electron microprobe results. In comparison, NG-derived Cl data are 2-5 relative % higher than the CIC data (Tab. 2). The Br contents obtained by the NG method for PY-1, JH-128 and JH-053 are 20-30 relative % higher than those

obtained by CIC and 17 relative % lower than those obtained by INAA (PY-1 only) (Tab. 2). This scatter is partly a function of the different standardization protocols (see methods) but may also indicate that the separation of the Br from the dominating Cl peak during ion chromatography was not perfect (see above). Note, however, that CIC results for other reference materials such as granite and basalt are within the reported literature values (Tab.2).

Iodine concentrations obtained by the NG and CIC methods are within 24 relative % of one another for JH53 and consistent for sample JH128 in which I was below the CIC detection limit. However, the I concentration obtained by the NG method for sample PY-1 is about twice the one obtained by CIC (Tab. 2).

The SIMS data indicate that small-scale heterogeneities in Br and I concentrations are present in many of the investigated samples (section 4.3). Therefore, sample heterogeneity may contribute to the different results obtained from the different techniques. The sample masses of ~10 mg for CIC and 5-30 mg for the NG method overlap and sample duplicates analyzed by the NG method were reproduced at the 3% level for Cl, 0.3-9% for Br and 1-21% for I, with the greatest heterogeneity indicated for the duplicate pair including the smallest sample aliquot (Tab. 2). Further work to cross-calibrate these techniques is desirable. However, given the demonstrable heterogeneity of the sample material (and the orders of magnitude variation in halogen abundances in natural materials), these results provide confidence that the CIC results reported below are meaningful.

4.2. Bulk halogen (Cl, F, Br, I) contents

The EPMA and CIC data indicate that the samples contain between 1.9 and 2.5 wt% Cl and generally < 0.3 wt% F (Tab. 3). An exceptionally high F-content of 1 wt% was determined in sample JH-001, where fluorite occurs as a gangue mineral. Although pyromorphite (JH-101) and mimetite (JH-017) contain fluoro-phosphohedyphane zones, they do not have

exceptionally high bulk F contents, as these zones are only up to 100 µm thick and are therefore too small to influence the bulk data. Bulk Br contents are highly variable and range from 0.3 to 20 µg g^{-1}, as do I contents, which vary from < 0.1 to 26 µg g^{-1} (Tab. 3).

The contents of F, Br and I correlate strongly with the major element composition (Fig. 5): pyromorphite samples (P# > 0.6) reach high levels of F and show only low Br contents (< 5 µg g^{-1}). In contrast, mimetite (P# < 0.4) and vanadinite reach the highest Br contents but contain only little F (generally < 500 µg g^{-1}) and I (< 2 µg g^{-1}). Mimetite with phosphohedyphane zones shows the same systematics as mimetite, and pyromorphite with phosphohedyphane zones the same as pyromorphite (Fig. 5).

4.3. Spatially resolved halogen data

The samples analyzed by SIMS and EPMA do not show large variations on the A site, with P# (P/P+As+V) in pyromorphites ranging from 0.98 to 1 and between 0.0 to 0.2 in mimetites. The visible zonation in BSE images (Figs. 6 and 7) is mainly due to variations in Pb and Ca (Tab. 4).

Type-A samples do not show any obvious zonation patterns in BSE images. The example shown in Fig. 6a has a constant Pb# of 1.00 and shows increasing Br/I from core (0.4) to rim (5.0), due to increasing Br contents. A similar trend is visible in the F/Cl ratio (0.001 to 0.004), since Cl slightly decreases towards the rim, whereas F increases (Fig. 6a).

Type B samples (Fig. 6b) show dark and relatively Ca-rich areas (Ca# 0.2-0.25) and brighter, relatively Ca-poor areas (Ca# 0.01). In the example shown, the brightest area has the lowest F/Cl (0.01), but the highest Br/I ratio (0.11) due to relatively low F (200 µg g^{-1}) and I (15 µg g^{-1}) contents. In the remaining parts of this sample, non-systematic variations of all four halogens occur, with remarkably high I contents (up to 35µg g^{-1}) relative to Br (1-2 µg g^{-1}) (Fig. 6b).

Type C samples show clear halogen variations from internal (relatively old) to external (relatively younger) zones (Figs. 6c, 7a, b). In pyromorphite JH-118, F (from 400 to 17 µg g^{-1}), Br (from 2.3 to 0.6 µg g^{-1}) and I (from 2 to 0.08 µg g^{-1}) contents decrease from core to rim, resulting in increasing Br/I but decreasing F/Cl and Br/Cl ratios in the same direction (Fig. 6c). In pyromorphite JH-078, no systematic halogen variations from core to rim are evident and Br/Cl, Br/I and F/Cl ratios scatter in an unsystematic way (Fig. 7a). Halogen variations in mimetite JH-114 (Fig. 7b) are less compared to pyromorphites JH-118 (Fig. 6c) and JH-078 (Fig. 7a), whereas F, Br and I contents are relatively constant in most of the sample. A later overgrowth shows higher F and I but lower Br contents. This results in distinctly higher F/Cl and lower Br/I and Br/Cl ratios.

5. Discussion

Based on our results using different analytical techniques, we are able to distinguish different types of halogen incorporation (i) into different PyGMs in general, and (ii) into specific zones of individual crystals.

5.1. Crystal chemical controls on the incorporation of F, Br and I in pyromorphite-group minerals

The experimental study of Wondratschek (1963) showed that the incorporation of Cl, F and Br into PyGM is thermodynamically stable. In his study, Cl-, F-, and Br-PyGM endmembers were synthesized, but the synthesis of the I-pyromorphite endmember was not successful (Wondratschek, 1963). In natural PyGM, Cl is by far the most abundant halogen (we found a minimum concentration of 1.9 wt% in our samples), probably because Cl is the dominant halogen in basically all natural fluids (Cicerone, 1981; Göb et al., 2013; Neal et al., 2010). Flis et al. (2011) synthesized a number of solid solution compositions of the pyromorphite-

mimetite series with variable P/As ratios. The P/As ratio of initial fluid and final solid composition was identical which implies that no fractionation of P and As occurs between fluid and solid phases. In other words, PyGM P/As ratios reflect the P/As ratio of the fluid they crystallized from. In the following, we assume that this is also true for the halogens, but we stress that this is just an assumption. We believe that this assumption is reasonable, as the halogens (except for Cl) are trace elements in natural fluids and, hence, Henry's law applies. Hence, we suggest that the relation of halogen content and major element composition of the analyzed PyGM sheds light on the relative preferred incorporation of the different halogens into the different PyGMs, although the actual abundance of the halogens in the PyGM-forming fluid is unknown.

The halogen site of a Ca-poor PyGM is preferentially occupied by Cl relative to F, since compositions close to Pb_5A_3L have larger unit cell dimensions than compositions such as $Ca_2Pb_3A_3L$, and since larger unit-cell dimensions favor the incorporation of the halogen with the larger ionic radius (Markl et al., 2014; Pasero et al., 2010). This explains why hedyphane samples (Ca-rich compared to the "standard" PyGM), which have smaller unit-cell dimensions, incorporate greater amounts of F than, e.g., pyromorphite or mimetite. This is supported by the occurrence of phosphohedyphane (Ca-rich), which is the only naturally occurring F-dominated endmember (Kampf and Housley, 2011; Pasero et al., 2010). It is also illustrated by sample JH-127, in which the highest F content correlates with the highest Ca# (Fig. 6b).

On the other hand, the highest I content (the halogen with the largest ionic radius) was also detected in hedyphane zones (Tab. 4) which implies that halogen incorporation is not only dependent on the occupation of the Pb-Ca site in the PyGM crystal. Furthermore, we observed that the degree of Br and I substitution correlates with the P/(P+As) ratio of the PyGMs (Fig. 5, 9): higher P/(P+As) ratios favor substitution by I. The explanation for the observed data is,

however, difficult, and simple crystallographic arguments do not suffice. Arsenic (As^{5+}) has an effective ionic radius of 0.335 Å and vanadium (V^{5+}) of 0.355 Å, whereas phosphorous (P^{5+}) has an ionic radius of only 0.17 Å (Flis et al., 2010; Shannon, 1976). Thus, mimetite and vanadinite have similar and larger unit cell volumes than pyromorphite, correlating with significantly longer B-O (B= As, V, P) bond lengths that increase linearly with cell volume (e.g., Dai and Hughes, 1989; Okudera, 2013; Shannon, 1976). Furthermore, the polyhedral volume of the Cl site in the $Pb2_6$ octahedron is smaller in pyromorphite (40.1 $Å^3$) compared to mimetite (41.9 $Å^3$) and vanadinite (42.0 $Å^3$) (Okudera, 2013). Hence, Br (which has a smaller ionic radius than I) should be preferentially incorporated (relative) in pyromorphite and I preferentially incorporated in mimetite and vanadinite. However, the opposite is observed: pyromorphite has higher I concentrations (Fig. 8).

If, crystallography does not explain the observed incorporation patterns, they could be a function of the composition of the fluid from which the PyGMs crystallize. In this case, we would have to assume that fluid composition alternates (see e.g., Fig. 7b) between P-dominated/I-rich and As-dominated/Br-rich endmembers. Based on the experiments of Flis et al. (2011) which imply that the PyGM mirrors the composition of the coexisting fluid the resulting minerals would be I-rich pyromorphite and Br-rich mimetite. This is the case in sample JH 114 (Fig. 7b), where the core is Br-rich mimetite, whereas the outer rim is I-rich pyromorphite. This sample clearly records a drastic change of the fluid chemistry with time. Arsenic in the fluid mainly derives from weathering of vein and host rock minerals (Basu and Schreiber, 2013), whereas the primary P source has microbial origin, i.e., plant litter from topsoil horizons (Burmann et al., 2013). This distinction would imply that different fluid pathways of different initial fluid sources would lead to either pyromorphite or mimetite precipitation. The positive correlation of pyromorphite with I and of mimetite with Br indicates that not only P and As have different sources, but also I and Br are derived from

different reservoirs. This is surprising, as both halogens are believed to be "biophilic" (Fuge, 1988), and we have no explanation so far for this observation. However, not only the initial source, but also the amount of available As or P at the time of PyGM formation determines which PyGM precipitates.

5.2. Possible parameters influencing formation of pyromorphite-group minerals

Minor variations of the major element composition in single PyGM crystals can be explained by relatively constant boundary conditions during their formation. It seems unlikely to us that factors such as weathering of the host rock or fluid pathways change abruptly on such relatively short time scales.

However, trace elements are more prone to small scale processes in the environment and compositional zonation provides details about the crystal's formation environment and the evolution of the environmental parameters. This is comparable to zoned crystals in magmatic, metamorphic and hydrothermal systems (Boyce and Hervig, 2009; Harlov et al., 2005; Webster and Piccoli, 2015).

The composition of a mineral in equilibrium with a fluid is determined by external physico-chemical parameters such as temperature, pressure and fluid composition. Due to the shallow formation depth of the PyGM, temperature and pressure can be assumed to be relatively constant for individual crystals and thus, the fractionation factor for individual elements between fluid and mineral should be relatively constant throughout the crystallization of individual mineral aggregates. For example, it is well known that the temperature in shallow underground workings at dozens to a hundred meters' depth is basically constant and is identical to the annual mean temperature at the surface. The effect of temperature may only be important when different localities are compared. For example the mean annual temperature in the Rhine valley is close to 20°C while the highest Schwarzwald peaks have a mean annual temperature of 5°C.

We suggest, that the halogen variations within single PyGM crystals and aggregates reflect the compositional evolution of the fluid from which they precipitated. The composition of fluids from which secondary/supergene mineral phases are formed within the oxidation zone of ore deposits are initially governed by the composition of the precipitation. However, halogen input by rainfall is not a major contributor to halogen concentrations in the soil or vegetation (Lovett et al., 2005), but the amount of water that is available to leach rocks has an influence on the process of chemical weathering of minerals (Carroll, 2012). If the principle of lower fluid/rock ratios resulting in lower release rate, but higher halogen concentrations in the fluid (Burisch et al., 2016; Huang et al., 1986) is applied to halogen release by weathering of minerals, higher rainfall rates lead to a decrease in halogen concentrations of the fluid, i.e. the soil solution, which in turn results in variable halogen content among distinct growth zones of PyGM.

5.3. Halogens as a tracer- halogen variations independent of major element composition

Pyromorphite and mimetite crystals can be strongly zoned with respect to their halogen contents (Figs. 6a-c, 7a, b). Since zoning can be found in crystals with a constant major element composition (P# and Ca#), exclusively crystallographic reasons can be excluded and an additional process needs to be invoked. Individual growth zones in PyGM have been interpreted to represent single episodes of fluid flow and related weathering reactions (e.g., Frost et al. 2007; Markl et al. 2014), and it has been shown that there are still active processes of PyGM crystallization on the walls of some underground workings and in medieval dumps (Burmann et al. 2013). Thus, small variations in the environmental conditions during PyGM formation, such as availability of halogens or other physico-chemical parameters, can affect halogen incorporation.

Potential halogen sources for PyGM formation include soil, rock and rain water. The halogen contents in these environmental components are known in very different detail and vary greatly (Fig. 9, Tab. 5). In general, on earth F and Cl have similar abundance (Kabata-Pendias 2011), but Cl is the dominant halogen in different types of waters, rocks and soils (similar as in PyGM) although some rock types like, e.g. evolved leucogranites contain more F than Cl; Tab. 5.

The highest Cl concentrations in surface waters are observed in seawater (18800 mg L^{-1}) and geothermal waters (1070 mg L^{-1}; Tab. 5). Rain and creek water contain Cl concentrations between 0.07 and 8.16 mg L^{-1}. In soils (depending on soil type and sampling depth), Cl concentrations are highly variable, with maximum Cl concentrations (up to 1200 mg kg^{-1}) in the humus layer of a forest soil (Tab. 5). Whole rock analyses from various igneous, metamorphic and sedimentary rock types show variable Cl concentrations, but are similar to the range observed in the soils (Tab. 5).

Comprehensive data sets that include Cl, F, Br and I content for the different geochemical reservoirs are sparse (Tab. 5). However, different reservoirs can be distinguished according to their Br/Cl, I/Cl and F/Cl ratio, (Fig. 9 a-c). The range of halogen ratios in PyGM compared to other known rocks, minerals and fluids shows that the Br/Cl ratios are notably lower in PyGM (Fig. 9 a-c), suggesting that Br is preferentially excluded from PyGM formation relative to Cl. The low Br/Cl ratios of PyGM partly overlap with those of F-apatite and to some extend with mica, mine and thermal waters (Fig. 9 a). Considering Br/Cl vs I/Cl ratios mimetite data fall in the amphibole field (Fig. 9 b), whereas pyromorphites, phosphoheyphanes and vandadinites do not overlap with any of the known data. One phosphohedyphane outlier lies within the marine pore fluids reservoir due to extremely high Br and I concentrations (Fig. 9 b), reflecting a possible organic contamination. When comparing F/Cl and I/Cl ratios, PyGM ratios partly overlap with amphibole, Cl-apatite and OH-apatite (Fig. 9 c). However, F/Cl

ratios of PyGM are distinctly lower compared to the other reservoirs, showing that the main distinctive feature are not I/Cl ratios but Br/Cl and F/Cl ratios (Fig. 9 a-c). Vanadinite has a F/Cl ratio comparable to seawater but an orders of magnitude higher I/Cl ratio (Fig. 9c).

The variations in halogen concentrations within and between the different geochemical reservoirs are attributed to a combination of complex abiotic and biotic processes. For example, the initial halogen composition of rain water is altered during seepage through the organic layer on top of the mineral soil, underlying mineral soil horizons and the host rock. Since (sub-) surface fluids are involved in the precipitation of PyGM, the halogen cycle in combination with the H_2O cycle has to be considered in order to understand variations in halogen availability during mineral formation.

The composition and seasonality of local rainfall is subordinately relevant due to its low halogen content; more important is its influence on the intensity of host rock alteration. The halogen composition of rainwater has been shown to fluctuate (Yuita et al., 2006). Absolute I concentrations in rain vary, depending on seasonal changes in rainfall frequency and intensity. Furthermore, rainwater in continental sites has lower halogen concentrations than coastal sites (Fuge 1988). Higher Br/Cl and I/Cl ratios were reported for inland areas (Fuge 1988, Neal et al. 2010) due to the relative enrichment of Br and I. After precipitation, the initial halogen content in the rainwater can be altered by vegetation, as plants commonly take up growth-relevant elements through the roots and thus increase the Cl concentrations in plant tissue and in throughfall relative to directly incident rainfall (Lovett et al. 2005; Oelmann et al. 2007). The impact of vegetation on throughfall is, however, rather negligible compared to other processes, since the Cl in the soil solution is primarily derived from weathering and not from rainfall (Lovett et al. 2005; Svensson et al. 2012). Halogens (Cl and Br) were regarded in the past as conservative tracers in fluid-involving processes in soils and upper crustal rocks (Öberg and Sandén, 2005). There is increasing evidence that halides serve as important

nutrients and are therefore actively being cycled by plants and microorganisms (Leri and Myneni, 2012; Öberg and Bastviken, 2012). Furthermore, evapotranspiration has an influence on downward water fluxes (Oelmann et al., 2007), since increased evapotranspiration leads to a limited transport of water in soil (Johansson et al., 2003 and references therein). Thus, it is likely that the effect of evaporation has an impact on halogen incorporation. Vegetation density and vegetation type may also influence halogen input into the soil to various extent (e.g., Låg and Steinnes, 1976).

A major halogen source for groundwater or soil water is rock weathering by leaching and dissolution of minerals, which strongly depends on the fluid/rock ratio (Carroll 2012). For example, feldspar dissolution experiments of Huang et al. (1986) revealed that elements are more rapidly released at higher fluid/rock ratios. However, even though a lower fluid/rock ratio may result in a lower release rate, it also results in higher halogen concentrations in the final fluid (Huang et al. 1986; Burisch et al. 2016), since lower fluid/rock ratios favor an increased retention time at the water-rock interface (Oliva et al. 2003). Microbial activity also influences the process of weathering and thus elemental release (Oliva et al. 2003; Wu et al. 2008), where the heterotrophic bacterial metabolism is pH-dependent. For example, a lower pH (e.g., due to nitrification processes) results in accelerated Ca release from minor phases in granite (Oliva et al. 2003; Wu et al. 2008). Consequently, variations in pH may also influence the release of halogens during biogeochemical weathering. However, soil-vegetation interactions are very complex. For example, thenvironmentale pH of the soil is dependent on, among others, host rock, type of vegetation, microbial activity, chemical processes within the soil and rainfall amount (Jenny 1941). Furthermore, vegetation and biological activity are also essential in defining the degree of weathering of the host rock (Sims 1990; Oades 1993; Seybold et al. 1999). Not only the vegetation, but also the thickness of the soil cover affects the weathering process, where a thin soil cover favors chemical weathering and the release of

545 halogens into the fluid (Oliva et al. 2003). At the same time, weathering results in the
546 formation of secondary minerals in the soil such as pedogenic oxides (Fe- and Al-oxides and
547 hydroxides) and clay minerals. These minerals are able to adsorb halides, thereby potentially
548 further altering the halogen composition in the fluid (Nodvin et al. 1986; Loganathan et al.
549 2007). FeOOH · nH2O strongly incorporates halogens into its structure, e.g., up to wt% Cl
550 and some ppm of I.

551 ## 6. Implications

552 Halogen concentrations in PyGM crystals from different localities, of various bulk
553 compositions and between specific zones in single crystals are controlled by changes in the
554 physico-chemical conditions during their formation (e.g., composition of the fluid,
555 temperature variations). Furthermore, crystal chemical effects may have an influence, but
556 their exact effect is not completely understood. Fluid-chemical and possibly crystallographic
557 effects can lead to variable halogen incorporation in different types of PyGM (pyromorphite,
558 mimetite, vanadinite). Thus, halogen ratios of different PyGM may be used as fluid monitors,
559 since it was shown that the halogens are preferentially incorporated into specific PyGM.
560 Further studies, aimed at each respective process, are needed to understand and correlate the
561 zonation to individual processes. We therefore suggest interdisciplinary studies that not only
562 take into account abiotic aspects of mineral growth, but also potential biological influences on
563 the weathering (and formation) of PyGM in near-surface environments. Furthermore,
564 experimental work on mineral-fluid partitioning behavior for the different halogens with
565 respect to mineral type is essential for further understanding halogen incorporation into
566 PyGM. The environmental importance of this mineral group due to incorporation and removal
567 of toxic elements from the environment requires a more detailed investigation. Moreover,
568 PyGM are of further interest as they incorporate significant amounts of Cl, thus depriving the
569 fluid of Cl, which is an important complexing agent for many toxic elements. This in turn

570 implies that the mobility of these toxic elements is reduced, not only by direct incorporation
571 into PyGM, but also by removal of Cl from the fluid and thus decreasing their mobility.

572

573 **Acknowledgements**

574 We are grateful to Thomas Wenzel for his invaluable help with the electron microprobe.
575 Simone Schafflick is thanked for the sample preparation. Further thank goes to Bernd
576 Steinhilber, who helped to develop the ideal method for the analyses. Axel Schmitt is thanked
577 for providing the Macusani glass sample. This research was funded by the German Research
578 Foundation (DFG) Grant No. MA 2135/23-1; OE 516/8-1. M. A. Kendrick was supported by
579 an Australian Research Council Future Fellowship (FT13 0100141). Furthermore, we would
580 like to thank the Editor Don Baker, the Associate Editor Andrew Madden and two anonymous
581 Reviewers for their constructive feedback which improved this manuscript significantly.

582

583

584 Bajda, T. (2010) Solubility of mimetite Pb5 (AsO4) 3Cl at 5–55 C. Environmental Chemistry, 7(3),
585 268-278.
586 Basta, N., and McGowen, S. (2004) Evaluation of chemical immobilization treatments for reducing
587 heavy metal transport in a smelter-contaminated soil. Environmental pollution, 127(1), 73-82.
588 Basu, A., and Schreiber, M.E. (2013) Arsenic release from arsenopyrite weathering: insights from
589 sequential extraction and microscopic studies. Journal of hazardous materials, 262, 896-904.
590 Behne, W. (1953) Untersuchungen zur Geochemie des Chlor und Brom. Geochimica et
591 Cosmochimica Acta, 3(4), 186-215.
592 Biester, H., Keppler, F., Putschnew, A., Martinez-Cortizas, A., and Petri, M. (2004). Halogen
593 retention, organohalogens, and the role of organic matter decomposition on halogen
594 enrichment in two Chilean peat bos. Environmental science & technology, 38(7), 1984-1991.
595 Biester, H., Hemmerich, S. and Petri, M. (2006). Halogens in porewater of peat bogs – the role of peat
596 decomposition and dissolved organic matter. Biogeosciences Discussions, 2(5), 1457-1486.
597 Böhlke, J.K., and Irwin, J.J. (1992) Brine history indicated by argon, krypton, chlorine, bromine, and
598 iodine analyses of fluid inclusions from the Mississippi Valley type lead-fluorite-barite
599 deposits at Hansonburg, New Mexico. Earth and Planetary Science Letters, 110(1), 51-66.
600 Boyce, J.W., and Hervig, R.L. (2009) Apatite as a monitor of late-stage magmatic processes at Volcán
601 Irazú, Costa Rica. Contributions to Mineralogy and Petrology, 157(2), 135.
602 Brook, E.J., Harder, S., Severinghaus, J., Steig, E.J., and Sucher, C.M. (2000) On the origin and
603 timing of rapid changes in atmospheric methane during the last glacial period. Global
604 Biogeochemical Cycles, 14(2), 559-572.

Burisch, M., Marks, M.A., Nowak, M., and Markl, G. (2016) The effect of temperature and cataclastic deformation on the composition of upper crustal fluids—An experimental approach. Chemical Geology, 433, 24-35.

Burmann, F., Keim, M.F., Oelmann, Y., Teiber, H., Marks, M.A., and Markl, G. (2013) The source of phosphate in the oxidation zone of ore deposits: Evidence from oxygen isotope compositions of pyromorphite. Geochimica et Cosmochimica Acta, 123, 427-439.

Carroll, D. (2012) Rock weathering. Springer Science & Business Media.

Cicerone, R.J. (1981) Halogens in the atmosphere. Reviews of Geophysics, 19(1), 123-139.

Dai, Y., Hughes, J., and Moore, P. (1991) The crystal of mimetite and clinomimetite, Pb 5 (AsO 4) 3 Cl. The Canadian Mineralogist, 29(2), 369-376.

Dai, Y., and Hughes, J.M. (1989) Crystal structure refinements of vanadinite and pyromorphite. The Canadian Mineralogist, 27(2), 189-192.

Dennen, W.H. (1960) Principles of mineralogy. Ronald Press Company.

Eaton, J.S., Likens, G.E., and Bormann, F.H. (1973) Throughfall and stemflow chemistry in a northern hardwood forest. The Journal of Ecology, 495-508.

Eby, G.N. (1990) The A-type granitoids: a review of their occurrence and chemical characteristics and speculations on their petrogenesis. Lithos, 26(1-2), 115-134.

Ehlers, J., and Gibbard, P.L. (2004) Quaternary glaciations-extent and chronology: Part I: Europe. Elsevier.

Fehn, U., Snyder, G., and Egeberg, P.K. (2000) Dating of Pore Waters with ¹²⁹I: Relevance for the Origin of Marine Gas Hydrates. Science, 289(5488), 2332-2335.

Fehn, U., Snyder, G.T., and Muramatsu, Y. (2007) Iodine as a tracer of organic material: 129I results from gas hydrate systems and fore arc fluids. Journal of Geochemical Exploration, 95(1), 66-80.

Flis, J., Borkiewicz, O., Bajda, T., Manecki, M., and Klasa, J. (2010) Synchrotron-based X-ray diffraction of the lead apatite series Pb10 (PO4) 6Cl2–Pb10 (AsO4) 6Cl2. Journal of synchrotron radiation, 17(2), 207-214.

Flis, J., Manecki, M., and Bajda, T. (2007) Solubility of pyromorphite-mimetite solid solutions at 5-65 degrees C: Variability of thermodynamic stability of minerals from pyromorphite-mimetite series at 5-65 degrees C. Geochimica et Cosmochimica Acta, 71, p. A285-A285.

Flis, J., Manecki, M., Badja, T. (2011) Solubility of pyromorphite Pb5 (PO4) 3Cl–mimetite Pb5 (AsO4) 3Cl solid solution series. Geochimica et Cosmochimica Acta, 75(7), 1858-1868.

Förtsch, E., and Wondratschek, H. (1965) Zur Kristallchemie der Minerale der Pyromorphit-Gruppe. Naturwissenschaften, 52(8), 182-182.

Fuge, R. (1988) Sources of halogens in the environment, influences on human and animal health. Environmental Geochemistry and Health, 10(2), 51-61.

Fuge, R., and Johnson, C.C. (1986) The geochemistry of iodine — a review. Environmental Geochemistry and Health, 8(2), 31-54.

Gao, S., Luo, T.-C., Zhang, B.-R., Zhang, H.-F., Han, Y.-w., Zhao, Z.-D., and Hu, Y.-K. (1998) Chemical composition of the continental crust as revealed by studies in East China. Geochimica et Cosmochimica Acta, 62(11), 1959-1975.

Gerke, T.L., Scheckel, K.G., and Schock, M.R. (2009) Identification and distribution of vanadinite (Pb5 (V5+ O4) 3Cl) in lead pipe corrosion by-products. Environmental science & technology, 43(12), 4412-4418.

Gieskes, J.M., and Mahn, C. (2007) Halide systematics in interstitial waters of ocean drilling sediment cores. Applied Geochemistry, 22(3), 515-533.

Göb, S., Loges, A., Nolde, N., Bau, M., Jacob, D.E., and Markl, G. (2013) Major and trace element compositions (including REE) of mineral, thermal, mine and surface waters in SW Germany and implications for water–rock interaction. Applied Geochemistry, 33, 127-152.

Hålenius, U., Hatert, F., Pasero, M., and Mills, S.J. (2017) New minerals and nomenclature modifications approved in 2017. Mineralogical Magazine, 81(5), 1279-1286.

Harlov, D.E. (2015) Apatite: A fingerprint for metasomatic processes. Elements, 11(3), 171-176.

Harlov, D.E., Wirth, R., and Förster, H.-J. (2005) An experimental study of dissolution–reprecipitation in fluorapatite: fluid infiltration and the formation of monazite. Contributions to Mineralogy and Petrology, 150(3), 268-286.

Hautmann, S., and Lippolt, H. (2000) 40Ar/39Ar dating of central European K–Mn oxides—a chronological framework of supergene alteration processes during the Neogene. Chemical Geology, 170(1-4), 37-80.

Herrmann, A.G. (1980) Bromide distribution between halite and NaCl-saturated seawater. Chemical Geology, 28, 171-177.

Hofmann, B., and Eikenberg, J. (1991) The Krunkelbach uranium deposit, Schwarzwald, Germany; correlation of radiometric ages (U-Pb, U-Xe-Kr, K-Ar, 230 Th-234 U). Economic Geology, 86(5), 1031-1049.

Huang, W., Bishop, A., and Brown, R. (1986) The effect of fluid/rock ratio on feldspar dissolution and illite formation under reservoir conditions. Clay Minerals, 21(4), 585-601.

Janicka, U., Bajda, T., and Manecki, M. (2012) Synthesis and solubility of brompyromorphite Pb5 (PO4) 3Br. Mineralogia Polonica, 43(1-2), 129-135.

Johansson, E., Sandén, P., and Öberg, G. (2003) Organic chlorine in deciduous and coniferous forest soils in southern Sweden. Soil Science, 168(5), 347-355.

John, T., Scambelluri, M., Frische, M., Barnes, J.D., and Bach, W. (2011) Dehydration of subducting serpentinite: implications for halogen mobility in subduction zones and the deep halogen cycle. Earth and Planetary Science Letters, 308(1-2), 65-76.

Johns, W., and Huang, W. (1967) Distribution of chlorine in terrestrial rocks. Geochimica et Cosmochimica Acta, 31(1), 35-49.

Johnson, L., Burgess, R., Turner, G., Milledge, H., and Harris, J. (2000) Noble gas and halogen geochemistry of mantle fluids: comparison of African and Canadian diamonds. Geochimica et Cosmochimica Acta, 64(4), 717-732.

Kalt, A., Altherr, R., and Hanel, M. (2000) The Variscan basement of the Schwarzwald. European Journal of Mineralogy, 12, 1-43.

Kampf, A.R., and Housley, R.M. (2011) Fluorphosphohedyphane, Ca2Pb3 (PO4) 3F, the first apatite supergroup mineral with essential Pb and F. American Mineralogist, 96(2-3), 423-429.

Keim, M.F., and Markl, G. (2015) Weathering of galena: Mineralogical processes, hydrogeochemical fluid path modeling, and estimation of the growth rate of pyromorphite. American Mineralogist, 100(7), 1584-1594.

Kendrick, M., and Phillips, D. (2009) New constraints on the release of noble gases during in vacuo crushing and application to scapolite Br–Cl–I and 40Ar/39Ar age determinations. Geochimica et Cosmochimica Acta, 73(19), 5673-5692.

Kendrick, M., Phillips, D., Wallace, M., and Miller, J.M. (2011) Halogens and noble gases in sedimentary formation waters and Zn–Pb deposits: A case study from the Lennard Shelf, Australia. Applied Geochemistry, 26(12), 2089-2100.

Kendrick, M.A. (2012) High precision Cl, Br and I determinations in mineral standards using the noble gas method. Chemical Geology, 292, 116-126.

Kendrick, M.A., Arculus, R., Burnard, P., and Honda, M. (2013) Quantifying brine assimilation by submarine magmas: Examples from the Galápagos Spreading Centre and Lau Basin. Geochimica et Cosmochimica Acta, 123, 150-165.

Kendrick, M.A., and Burnard, P. (2013) Noble gases and halogens in fluid inclusions: A journey through the Earth's crust. The noble gases as geochemical tracers, p. 319-369. Springer.

Kendrick, M.A., D'Andres, J., Holden, P., and Ireland, T. (2018) Halogens (F, Cl, Br, I) in Thirteen USGS, GSJ and NIST International Rock and Glass Reference Materials. Geostandards and Geoanalytical Research.

Kendrick, M.A., Honda, M., and Vanko, D.A. (2015) Halogens and noble gases in Mathematician Ridge meta-gabbros, NE Pacific: implications for oceanic hydrothermal root zones and global volatile cycles. Contributions to Mineralogy and Petrology, 170(5-6), 43.

Kendrick, M.A., Jackson, M.G., Kent, A.J.R., Hauri, E.H., Wallace, P.J., and Woodhead, J. (2014) Contrasting behaviours of CO2, S, H2O and halogens (F, Cl, Br, and I) in enriched-mantle melts from Pitcairn and Society seamounts. Chemical Geology, 370, 69-81.

Kendrick, M.A., Kamenetsky, V.S., Phillips, D., and Honda, M. (2012) Halogen systematics (Cl, Br, I) in mid-ocean ridge basalts: a Macquarie Island case study. Geochimica et Cosmochimica Acta, 81, 82-93.

Knyazev, A., Chernorukov, N., and Bulanov, E. (2011) Phase diagram of apatite system Ca10 (PO4) 6Cl2–Pb10 (PO4) 6Cl2. Thermochimica acta, 526(1-2), 72-77.

716 Krám, P., Hruška, J., Wenner, B.S., Discoll, C.T., and Johnson, C.E. (1997) The biogeochemistry of
717 basic cations in two forest catchments with contrasting lithology in the Czech Republic.
718 Biogeochemistry, 37(2), 173-202.
719 Kusebauch, C., John, T., Barnes, J.D., Klügel, A., and Austrheim, H.O. (2015a) Halogen element and
720 stable chlorine isotope fractionation caused by fluid–rock interaction (Bamble Sector, SE
721 Norway). Journal of Petrology, 56(2), 299-324.
722 Kusebauch, C., John, T., Whitehouse, M.J., and Engvik, A.K. (2015b) Apatite as probe for the halogen
723 composition of metamorphic fluids (Bamble Sector, SE Norway). Contributions to
724 Mineralogy and Petrology, 170(4), 34.
725 Låg, J., and Steinnes, E. (1976) Regional distribution of halogens in Norwegian forest soils.
726 Geoderma, 16(4), 317-325.
727 Leri, A.C., and Myneni, S.C. (2012) Natural organobromine in terrestrial ecosystems. Geochimica et
728 Cosmochimica Acta, 77, 1-10.
729 Lovett, G.M., Likens, G.E., Buso, D.C., Driscoll, C.T., and Bailey, S.W. (2005) The biogeochemistry
730 of chlorine at Hubbard Brook, New Hampshire, USA. Biogeochemistry, 72(2), 191-232.
731 Lyubetskaya, T., and Korenaga, J. (2007) Chemical composition of Earth's primitive mantle and its
732 variance: 1. Method and results. Journal of Geophysical Research: Solid Earth, 112(B3).
733 Markl, G., Marks, M.A., Holzäpfel, J., and Wenzel, T. (2014) Major, minor, and trace element
734 composition of pyromorphite-group minerals as recorder of supergene weathering processes
735 from the Schwarzwald mining district, SW Germany. American Mineralogist, 99(5-6), 1133-
736 1146.
737 Marks, M.A., Kendrick, M.A., Eby, G.N., Zack, T., and Wenzel, T. (2017) The F, Cl, Br and I
738 Contents of Reference Glasses BHVO-2G, BIR-1G, BCR-2G, GSD-1G, GSE-1G, NIST SRM
739 610 and NIST SRM 612. Geostandards and Geoanalytical Research, 41(1), 107-122.
740 Marks, M.A., Wenzel, T., Whitehouse, M.J., Loose, M., Zack, T., Barth, M., Worgard, L., Krasz, V.,
741 Eby, G.N., and Stosnach, H. (2012) The volatile inventory (F, Cl, Br, S, C) of magmatic
742 apatite: An integrated analytical approach. Chemical Geology, 291, 241-255.
743 McCaffrey, M., Lazar, B., and Holland, H. (1987) The evaporation path of seawater and the
744 coprecipitation of Br (super-) and K (super+) with halite. Journal of Sedimentary Research,
745 57(5), 928-937.
746 Metz, R., and Richter, M. (1957) Die Blei-Zink-Erzgänge des Schwarzwaldes. Beihefte zum
747 Geologischen Jahrbuch, Beiheft 29, 277.
748 Morel, P., Von Blanckenburg, F., Schaller, M., Kubik, P.W., and Hinderer, M. (2003) Lithology,
749 landscape dissection and glaciation controls on catchment erosion as determined by
750 cosmogenic nuclides in river sediment (the Wutach Gorge, Black Forest). Terra Nova, 15(6),
751 398-404.
752 Muramatsu, Y., Doi, T., Tomaru, H., Fehn, U., Takeuchi, R., and Matsumoto, R. (2007) Halogen
753 concentrations in pore waters and sediments of the Nankai Trough, Japan: Implications for the
754 origin of gas hydrates. Applied Geochemistry, 22(3), 534-556.
755 Muramatsu, Y., Fehn, U., and Yoshida, S. (2001) Recycling of iodine in fore-arc areas: evidence from
756 the iodine brines in Chiba, Japan. Earth and Planetary Science Letters, 192(4), 583-593.
757 Muramatsu, Y., and Wedepohl, K.H. (1998) The distribution of iodine in the earth's crust. Chemical
758 Geology, 147(3-4), 201-216.
759 Neal, C., Robinson, M., Reynolds, B., Neal, M., Rowland, P., Grant, S., Norris, D., Williams, B.,
760 Sleep, D., and Lawlor, A. (2010) Hydrology and water quality of the headwaters of the River
761 Severn: Stream acidity recovery and interactions with plantation forestry under an improving
762 pollution climate. Science of the total environment, 408(21), 5035-5051.
763 Nriagu, J.O. (1973) Lead orthophosphates—III. Stabilities of fluoropyromorphite and
764 bromopyromorphite at 25° C. Geochimica et Cosmochimica Acta, 37(7), 1735-1743.
765 Öberg, G., and Bastviken, D. (2012) Transformation of chloride to organic chlorine in terrestrial
766 environments: variability, extent, and implications. Critical reviews in environmental science
767 and technology, 42(23), 2526-2545.
768 Öberg, G., and Sandén, P. (2005) Retention of chloride in soil and cycling of organic matter-bound
769 chlorine. Hydrological Processes: An International Journal, 19(11), 2123-2136.
770 Oelmann, Y., Kreutziger, Y., Temperton, V.M., Buchmann, N., Roscher, C., Schumacher, J., Schulze,
771 E.-D., Weisser, W.W., and Wilcke, W. (2007) Nitrogen and Phosphorus Budgets in

772 Experimental Grasslands of Variable Diversity. Journal of Environmental Quality, 36(2), 396-
773 407.
774 Okudera, H. (2013) Relationships among channel topology and atomic displacements in the structures
775 of Pb5 (B O4) 3Cl with B= P (pyromorphite), V (vanadinite), and As (mimetite). American
776 Mineralogist, 98(8-9), 1573-1579.
777 Palme, H., and O'Neill, H.S.C. (2003) Cosmochemical estimates of mantle composition. Treatise on
778 geochemistry, 2, 568.
779 Park Jr, C.F., and MacDiarmid, R.A. (1975) Ore deposits. W.H. Freeman and Co., San Francisco.
780 Pasero, M., Kampf, A.R., Ferraris, C., Pekov, I.V., Rakovan, J., and White, T.J. (2010) Nomenclature
781 of the apatite supergroup minerals. European Journal of Mineralogy, 22(2), 163-179.
782 Pfaff, K., Romer, R.L., and Markl, G. (2009) U-Pb ages of ferberite, chalcedony, agate,'U-mica'and
783 pitchblende: constraints on the mineralization history of the Schwarzwald ore district.
784 European Journal of Mineralogy, 21(4), 817-836.
785 Pichavant, M., Herrera, J.V., Boulmier, S., Joron, J.L., Juteau, M., Marin, L., Sheppard, S.M.F.,
786 Treuil, M., and Vernet, M. (1987) The Macusani glasses, SE Peru: evidence of chemical
787 fractionation in peraluminous magmas. Magmatic Process: Physicochemical Principles.
788 Geochem. Soc. Spec. Publ., 1, 359-373.
789 Redon, P.-O., Jolivet, C., Saby, N.P., Abdelouas, A., and Thiry, Y. (2013) Occurrence of natural
790 organic chlorine in soils for different land uses. Biogeochemistry, 114(1-3), 413-419.
791 Reich, M., and Vasconcelos, P.M. (2015) Geological and economic significance of supergene metal
792 deposits. Elements, 11(5), 305-310.
793 Roddick, J. (1983) High precision intercalibration of 40Ar-39Ar standards. Geochimica et
794 Cosmochimica Acta, 47(5), 887-898.
795 Ruby, M.V., Davis, A., and Nicholson, A. (1994) In situ formation of lead phosphates in soils as a
796 method to immobilize lead. Environmental Science & Technology, 28(4), 646-654.
797 Rudnick, R.L., and Shan, G. (2003) Composition of the continental crust. Treatise on geochemistry, 3,
798 659.
799 Schnetger, B., and Muramatsu, Y. (1996) Determination of halogens, with special reference to iodine,
800 in geological and biological samples using pyrohydrolysis for preparation and inductively
801 coupled plasma mass spectrometry and ion chromatography for measurement. Analyst,
802 121(11), 1627-1631.
803 Seelig, U., and Bucher, K. (2010) Halogens in water from the crystalline basement of the Gotthard rail
804 base tunnel (central Alps). Geochimica et Cosmochimica Acta, 74(9), 2581-2595.
805 Shannon, R.D. (1976) Revised effective ionic radii and systematic studies of interatomic distances in
806 halides and chalcogenides. Acta crystallographica section A: crystal physics, diffraction,
807 theoretical and general crystallography, 32(5), 751-767.
808 Siegel, F.R. (2002) Environmental geochemistry of potentially toxic metals. Springer.
809 Siemann, M.G., and Schramm, M. (2000) Thermodynamic modelling of the Br partition between
810 aqueous solutions and halite. Geochimica et Cosmochimica Acta, 64(10), 1681-1693.
811 Staude, S., Bons, P.D., and Markl, G. (2009) Hydrothermal vein formation by extension-driven
812 dewatering of the middle crust: An example from SW Germany. Earth and Planetary Science
813 Letters, 286(3-4), 387-395.
814 Teiber, H., Marks, M.A., Wenzel, T., Siebel, W., Altherr, R., and Markl, G. (2014) The distribution of
815 halogens (F, Cl, Br) in granitoid rocks. Chemical Geology, 374, 92-109.
816 Teiber, H., Scharrer, M., Marks, M.A., Arzamastsev, A.A., Wenzel, T., and Markl, G. (2015)
817 Equilibrium partitioning and subsequent re-distribution of halogens among apatite–biotite–
818 amphibole assemblages from mantle-derived plutonic rocks: Complexities revealed. Lithos,
819 220, 221-237.
820 Timmerman, M., and McCann, T. (2008) The Geology of Central Europe. Volume 1: Precambrian and
821 Palaeozoic.
822 Tomaru, H., Fehn, U., Lu, Z., Takeuchi, R., Inagaki, F., Imachi, H., Kotani, R., Matsumoto, R., and
823 Aoike, K. (2009) Dating of Dissolved Iodine in Pore Waters from the Gas Hydrate Occurrence
824 Offshore Shimokita Peninsula, Japan: 129I Results from the D/V Chikyu Shakedown Cruise.
825 Resource Geology, 59(4), 359-373.
826 Walter, B.F., Burisch, M., Fusswinkel, T., Marks, M.A.W., Steele-MacInnis, M., Wälle, M.,
827 Apukhtina, O.B., and Markl, G. (2018) Multi-reservoir fluid mixing processes in rift-related

hydrothermal veins, Schwarzwald, SW-Germany. Journal of Geochemical Exploration, 186, 158-186.

Walter, B.F., Burisch, M., and Markl, G. (2016) Long-term chemical evolution and modification of continental basement brines–a field study from the Schwarzwald, SW Germany. Geofluids, 16(3), 604-623.

Wang, L.-X., Ma, C.-Q., Zhang, C., Zhu, Y.-X., and Marks, M.A. (2018) Halogen geochemistry of I- and A-type granites from Jiuhuashan region (South China): Insights into the elevated fluorine in A-type granite. Chemical Geology, 478, 164-182.

Webster, J.D., and Piccoli, P.M. (2015) Magmatic apatite: A powerful, yet deceptive, mineral. Elements, 11(3), 177-182.

Whitfield, M., and Turner, D. (1979) Water–rock partition coefficients and the composition of seawater and river water. Nature, 278(5700), 132-137.

Wilson, T. (1975) Salinity and the major elements of seawater, Chemical Oceanography, 1 JP Riley, G. Skirrow, Academic, San Diego, Calif.

Wondratschek, H. (1963) Untersuchungen zur Kristallchemie der Blei-Apatite (Pyromorphite). Neues Jahrbuch für Mineralogie Abhandlungen, 99, 113-160.

Wong, G., and Brewer, P. (1974) Determination and distribution of Iodate in South-Atlantic waters. Journal of Marine Research, 32(1), 25-36.

Yuita, K., Kihou, N., Ichihasi, H., Yabusaki, S., Fujiwara, H., Kurishima, K., and Noda, T. (2006) Behavior of iodine in a forest plot, an upland field and a paddy field in the upland area of Tsukuba, Japan: Seasonal variations in iodine concentration in precipitation and soil water and estimation of the annual iodine accumulative amount in soil horizons. Soil science and plant nutrition, 52(1), 122-132.

Yuita, K., Shibuya, M., and Nozaki, T. (1978) The accumulation of bromine and iodine in Japanese soils. Abstract 11th Soil Science Congress Edmonton, Alberta, 260.

Table captions

Tab. 1 Information about the locality, mineralization type, host rock, methods used, crystal shape and basic mineralogy of all samples investigated.

Tab. 2 Internal reference material of samples JH-063, JH-128 and PY-1 characterized by different methods.

Tab. 3 All Combustion Ion Chromatography analyses and important EPMA data.

Tab. 4 All Secondary Ion Mass Spectrometry data and Cl reference values from the EPMA.

Tab. 5 Halogen data compilation in water, soil, rocks and vegetation, b.d.l. = below the detection limit.

Supplementary data table captions

ESM1 WDS analysis configuration used for the EMPA

ESM2 Concentrations used for calibration of the SIMS analyses and the resulting RIYs. The mean RIY for each element was applied to the analyses of the unknowns. 1σ standard deviation is given in parentheses.

Figure captions

Fig 1 Simplified geological overview of the Schwarzwald (SW Germany). Sample localities 1-23 (for more information refer to Tab. 1). Abbreviations: BLZ and BBZ = Badenweiler-Lenzkirch and Baden-Baden-Gaggenau Zones; CSGC and SSGC = Central and Southern Schwarzwald Gneiss Complexes. Map modified after Kalt et al. (2000).

Fig 2 Ternary diagram showing the sample classification of the pyromorphite-group minerals, n = number of analyzed samples. (a) All analyses of this study plotted in the ternary diagram pyromorphite-vanadinite-mimetite. The color-coding refers to the three distinguished crystal shapes. (b) The same analyses plotted in the trapezoid pyromorphite-phosphohedyphane-mimetite-hedyphane.

Fig 3 Halogen count rates and ratios using SIMS with (a) and (b) a pyromorphite sample and (c) and (d) with obsidian glass. Note the strong increase of count rates on the pyromorphite which is not present on the glass. However, the ratios on the pyromorphite are reasonably constant.

Fig 4 Method comparison between the electron microprobe analyses and the combustion ion chromatography with respect to the Cl-content (in wt%). The Cl-content of all CIC analyses and the appropriate Cl-content determined with the EPMA. Black circles show the three standard materials; JH-128 = mimetite, JH-053 = vanadinite, PY-1 = pyromorphite. Black vertical lines show the maximum Cl-content which can be theoretically incorporated into the

three endmembers. The color-coding refers to different host rocks and the shapes to different minerals. Vertical bars show the minimum and maximum detected Cl-content with the EPMA, each symbol represents the mean value. Vertical black bar = 1σ uncertainty EPMA, horizontal black bar = 1σ uncertainty CIC.

Fig 5 (a) Bromine vs iodine and (b) bromine vs. fluorine content, respectively, of all CIC analyses. The symbols refer to different minerals, the color-coding to the appropriate P# = P/(P+As+V). Error bars are smaller than the symbol size, with the exception of three samples, where the bars were shown accordingly. N = number of analyzed samples.

Fig 6 BSE images of (a) a macro- and microscopic non-zoned crystal, (b) a patchy zoned crystal and (c) a crystal with growth zoning combined with spatially resolved SIMS halogen data. Halogen ratios and absolute element concentrations are shown. Black vertical bars show average 1σ uncertainties of all measurements. Variations in gray scale in the BSE images are due to variations in Pb content.

Fig 7 BSE images of crystals with a distinct growth zoning (a+b) combined with spatially resolved SIMS halogen data. Halogen ratios and absolute element concentrations are shown. Black vertical bars show average 1σ uncertainties of all measurements. Variations in gray scale in the BSE images are due to variations in Pb content.

Fig 8 Bromine (a) and iodine (b) incorporation in PyGM, data based on all CIC and SIMS analyses. Abbreviations: pym= pyromorphite, mim= mimetite; P# = P/(P+As+V); Pb# = Pb/(Pb+As). Small blue symbols refer to minor element content and transition to large red symbols to higher element content. Dashed lines mark samples with either F or Cl as dominating halogen. (a) Increasing Br content with decreasing P# and slightly increasing Pb#. (b) Increasing I content with increasing P# and slightly decreasing Pb#.

Fig 9 The halogen systematics in different reservoirs (a) Br/Cl ratios of several rock, mineral, soil and water types. Bold minerals = data of this study. Pyromorphite, mimetite and phosphohedyphane ratios plot between Durango F-apatite and metamorphic Cl- and OH-apatite and lie below water and soil analyses. (b) Br/Cl plotted against I/Cl shows that mimetite data partly overlaps with the amphibole field, whereas pyromorphite plots between the Durango F-apatite field and the amphibole field. (c) F/Cl plotted against I/Cl shows that the data of this study plots between sedimentary pore fluids and apatite and amphibole analyses. Grey fields indicate several reservoirs, based on literature data, analyzed with different analytical techniques. NG = noble gas, IC = Ion Chromatography, SIMS = Secondary Ion Mass Spectrometry, ICP-MS = Inductively Coupled Plasma-Mass Spectrometry, TXRF = Total Reflection X-ray Fluorescence Spectroscopy. [1]Wang et al. (2018), [2]Burisch et al. (2016), [3]Behne (1953), [4]Kusebauch et al. (2015a), IC, ICP-MS, [5]Kendrick (2012), NG, [6]Kendrick and Burnard (2013), [7]Teiber et al. (2014), EPMA, TXRF, [8]Marks et al. (2012), SIMS, [9]Kusebauch et al. (2015b), SIMS, [10]Låg and Steinnes (1976), [11]Seelig and Bucher (2010), [12]Göb et al. (2013), samples from Germany, [13]Neal et al. (2010), samples from the UK, [14]Kendrick et al. (2011), [15]Fehn et al. (2000), [16]Fehn et al. (2007), [17]Fehn et al. (2007), [18]Muramatsu et al. (2001), [19]Muramatsu et al. (2007), [20]Gieskes and Mahn (2007), [21]Tomaru et al. (2009), [22]Kendrick et al. (2012), [23]McCaffrey et al. (1987), [24]Fuge and Johnson (1986), [25]Herrmann (1980), [26]Siemann and Schramm (2000), [27]Böhlke and Irwin (1992), [28]Kendrick et al. (2014), [29]Palme and O'Neill (2003), [30]Lyubetskaya and Korenaga (2007), [31]Rudnick and Shan (2003), [32]Biester et al. (2006), [33]Biester et al. (2004).

This is a preprint, the final version is subject to change, of the American Mineralogist (MSA)
Cite as Authors (Year) Title. American Mineralogist, in press.
DOI: https://doi.org/10.2138/am-2019-7068

No	Locality	Samples	Position a.NN	Coordination (UTM)	Host Rock	Mineralization type	Method			zoned	Shape	#Ca	#P	Color	Mineral
							SIMS	CIC	EPMA						
1	Silberbrünnle	JH-078	515	32 U 432271 5365312	gneiss	qtz-ccp-gn-fhl	x		x	x	crystalline	0.13	0.95	green	pym
2	Clara	JH-087	630	32 U 443346 5359394	gneiss	brt-fl-qtz-gn-fhl-ccp		x			crystalline	0.04	1.00	green	pym
2	Clara	JH-086	630	32 U 443346 5359394	gneiss	brt-fl-qtz-gn-fhl-ccp		x			crystalline	0.01	0.92	yellow-orange	pym
2	Clara	JH-089	630	32 U 443346 5359394	gneiss	brt-fl-qtz-gn-fhl-ccp		x			crystalline	0.00	0.02	orange	mim
3	Friedrich-Christian	JH-094	500	32 U 445999 5359392	gneiss	fl-qtz-gn-ccp		x			crystalline	0.01	1.00	green	pym
4	Herrensegen	JH-096	500	32 U 446018 5359411	gneiss	fl-qtz-gn-ccp	x		x	x	spherical	0.16	0.98	green	pym
4	Herrensegen	JH-092b	500	32 U 446018 5359411	gneiss	fl-qtz-gn-ccp	x		x	x	crystalline	0.10	0.99	green	pym
4	Herrensegen	JH-092a	500	32 U 446018 5359411	gneiss	fl-qtz-gn-ccp		x			crust	0.03	1.00	green	pym
4	Herrensegen	JH-097a	500	32 U 446018 5359411	gneiss	fl-qtz-gn-ccp		x			crystalline	0.00	1.00	green	pym
5	Erzengel Gabriel	JH-079	740	32 U 438778 5354736	gneiss	fl-brt-qtz-gn		x			crystalline	0.00	0.98	green	pym
6	Eichhalde Biberach	JH-101	260	32 U 426794 5354331	gneiss. granite	qtz-sid-fhl-gn-ccp		x			crust	0.19	1.00	green	pym-p.hed
7	Michael im Weiler	JH-076	370	32 U 423454 5356116	gneiss. granite	brt-qtz-gn-sph-nat.As		x			crystalline	0.00	0.15	orange	mim
7	Michael im Weiler	JH-074	370	32 U 423454 5356116	gneiss. granite	brt-qtz-gn-sph-nat.As		x			crust	0.00	0.82	orange	pym
7	Michael im Weiler	JH-077	370	32 U 423454 5356116	gneiss. granite	brt-qtz-gn-sph-nat.As		x			crystalline	0.00	0.00	yellow	mim
8	St. Josefi	JH-102	270	32 U 422415 5345980	gneiss	brt-qtz-gn-sph		x			crystalline	0.00	0.52	green	mim
9	Silberloch	JH-113	460	32 U 419816 5337573	sandstone	brt-qtz-gn(-fhl)		x			crystalline	0.07	0.95	green	pym
9	Silberloch	JH-112	460	32 U 419816 5337573	sandstone	brt-qtz-gn(-fhl)		x			crystalline	0.02	0.93	yellow	pym
10	Gsprenggang	JH-048	1180	32 T 416907 5306385	gneiss. migmatite	qtz-gn-sph		x			spherical	0.02	1.00	green	pym
11	Willnau	JH-045	1120	32 T 417456 5304584	migmatite	qtz-brt-gn		x			crystalline	0.00	1.00	green	pym
12	Kammentobel	JH-122b_Q	1320	32 T 424654 5303177	migmatite	sid/goe-gn	x		x		crystalline	0.00	1.00	green	pym
12	Kammentobel	JH-122b_L	1320	32 T 424654 5303177	migmatite	sid/goe-gn	x		x		crystalline	0.00	1.00	green	pym

This is a preprint, the final version is subject to change, of the American Mineralogist (MSA)
Cite as Authors (Year) Title. American Mineralogist, in press.
DOI: https://doi.org/10.2138/am-2019-7068

12	Kammentobel	JH-119	1320	32 T 424654 5303177	migmatite	sid/goe-gn	x	x	x		crystalline	0.00	1.00	yellow-green	pym
12	Kammentobel	JH-118	1320	32 T 424654 5303177	migmatite	sid/goe-gn	x	x	x	x	crust	0.04	1.00	yellow-green	pym
12	Kammentobel	JH-117	1320	32 T 424654 5303177	migmatite	sid/goe-gn	x	x	x		crust	0.00	1.00	yellow-brown	pym
12	Kammentobel	JH-122	1320	32 T 424654 5303177	migmatite	sid/goe-gn		x			crystalline	0.00	1.00	green	pym
12	Kammentobel	JH-121	1320	32 T 424654 5303177	migmatite	sid/goe-gn		x		x	crystalline	0.03	1.00	yellow-green	pym
12	Kammentobel	JH-120	1320	32 T 424654 5303177	migmatite	sid/goe-gn		x			crust	0.00	1.00	green	pym
13	Klöpfe	JH-127a	700	32 T 409466 5303259	migmatite	qtz-brt-gn	x		x	x	crust	0.19	0.99	green-grey	pym-Pb p.hed
14	Anton Wieden	JH-058	820	32 T 417227 5299318	gneiss. granite	fl-brt-qtz-gn-sph(-ccp)		x			crystalline	0.01	0.04	yellow	mim
15	Pfingstsegen (Aitern)	JH-066	960	32 T 414854 5296459	schist	fl-brt-qtz-gn		x			crystalline	0.01	0.92	green	pym
16	Karlstollen	JH-036	660	32 T 401019 5294106	schist	qtz-brt-gn		x			spherical	0.05	0.05	orange	mim
17	Hausbaden	JH-017	610	32 T 400777 5293817	granite	qtz-brt-fl-gn(-sph-ccp)	x	x	x	x	spherical	0.01-0.40	0.05-0.99	orange	mim-p.hed
17	Hausbaden	JH-022	610	32 T 400777 5293817	granite	qtz-brt-fl-gn(-sph-ccp)		x			spherical	0.05	0.19	yellow	mim
17	Hausbaden	JH-020	610	32 T 400777 5293817	granite	qtz-brt-fl-gn(-sph-ccp)		x			crystalline	0.14	1.00	green	pym
18	Altemannfels	JH-128	610	32 T 400795 5293679	gneiss. sandstone	qtz-brt-gn	x		x		spherical			orange	mim
18	Altemannfels	JH-128b	610	32 T 400795 5293679	gneiss. sandstone	qtz-brt-gn	x		x	x	spherical	0.11	0.11	orange	mim
18	Altemannfels	JH-128e	610	32 T 400795 5293679	gneiss. sandstone	qtz-brt-gn		x			spherical	0.10	0.09	orange	mim
19	Wilhelminen-stollen	JH-028	620	32 T 400771 5293509	granite	qtz-brt-gn		x			crystalline	0.07	0.99	yellow-green	pym
19	Wilhelminen-stollen	JH-025	620	32 T 400771 5293509	granite	qtz-brt-gn		x			crystalline	0.10	0.89	orange	pym
21	Neuhoffnung	JH-129b	740	32 T 434064 5285952	gneiss. granite	fl-brt-qtz-dol-gn-sph-ccp	x		x	x	spherical	0.11	0.59	green-grey	mim
21	Neuhoffnung	JH-129a	740	32 T 434064 5285952	gneiss. granite	fl-brt-qtz-dol-gn-sph-ccp		x			spherical	0.03	0.43	orange	mim
21	Neuhoffnung	JH-011	740	32 T 434064 5285952	gneiss. granite	fl-brt-qtz-dol-gn-sph-ccp		x			crust	0.01	0.95	orange	pym
21	Neuhoffnung	JH-001	740	32 T 434064 5285952	gneiss. granite	fl-brt-qtz-dol-gn-sph-ccp		x			spherical	0.11	0.97	green	pym
21	Neuhoffnung	JH-007a	740	32 T 434064 5285952	gneiss. granite	fl-brt-qtz-dol-gn-sph-ccp		x			crystalline	0.00	0.99	green	pym
21	Neuhoffnung	JH-013	740	32 T 434064 5285952	gneiss. granite	fl-brt-qtz-dol-gn-sph-ccp		x			crystalline	0.03	1.00	green	pym

This is a preprint, the final version is subject to change, of the American Mineralogist (MSA)
Cite as Authors (Year) Title. American Mineralogist, in press.
DOI: https://doi.org/10.2138/am-2019-7068

21	Neuhoffnung	JH-002	740	32 T 434064 5285952	gneiss. granite	fl-brt-qtz-dol-gn-sph-ccp		x			crystalline	0.04	0.99	yellow-green	pym
21	Neuhoffnung	JH-016	740	32 T 434064 5285952	gneiss. granite	fl-brt-qtz-dol-gn-sph-ccp		x			crystalline	0.02	0.96	yellow	pym
20	Gottes Ehre. Urberg	JH-054	790	32 T 434060 5286155	gneiss. granite	fl-brt-qtz-dol-gn-sph-ccp		x			crystalline	0.00	0.04	red-brown	van
20	Gottes Ehre. Urberg	JH-005	790	32 T 434060 5286155	gneiss. granite	fl-brt-qtz-dol-gn-sph-ccp		x			spherical	0.01	0.01	yellow	mim
22	Segalen	JH-114	700	32 T 439729 5283604	rhyolite	fl-brt-qtz-gn	x		x	x	crust	0.08	0.24	yellow	mim
23	Osterzeitstollen	JH-053	1040	32 T 417712 5306115	gneiss. granite		x	x			crystalline	0.00	0.07	brown	van

This is a preprint, the final version is subject to change, of the American Mineralogist (MSA)
Cite as Authors (Year) Title. American Mineralogist, in press.
DOI: https://doi.org/10.2138/am-2019-7068

sample	mineral/ sample type	method	Cl (wt%)		Br (µg g^{-1})				I (µg g^{-1})			
			mean	1 sigma	mean	min	max	1 sigma	mean	min	max	1 sigma
JH 053	vanadinite	NG	2.68	0.1	19.3			0.3	0.72			0.01
		EPMA	2.34	0.07								
		CIC	2.37	0.07	13.13			0.8	0.86			0.3
		SIMS			26.86	23.99	34.27	3.35	0.58	0.35	0.80	0.17
JH 128	mimetite	NG	2.82	0.1	6.46			0.1	0.065			0.002
		EPMA	2.45	0.19								
		CIC	2.43	0.057	4.53			0.32	b.d.l.			b.d.l.
		SIMS			8.11	7.65	8.62	0.40	0.10	0.08	0.17	0.04
PY-1	pyromorphite	NG	2.8	0.1	2.15			0.03	3.2			0.1
		EPMA	2.54	0.19								
		INAA			2.3			0.12				
		CIC	2.46	0.06	1.63			0.15	1.34			0.1
		SIMS			0.82	0.66	1.02	0.13	3.09	1.70	3.83	0.84

This is a preprint, the final version is subject to change, of the American Mineralogist (MSA)
Cite as Authors (Year) Title. American Mineralogist, in press.
DOI: https://doi.org/10.2138/am-2019-7068

sample	EPMA								CIC													
	P	As	V	Pb	Ca	Cl mean	Cl min	Cl max	Cl			Br			F			I			Cl/Br ratio	σ (%)	F/Cl ratio	σ (%)	Br/I ratio	σ (%)
	a.p.f.u					wt%			wt%			μg g^{-1}														
JH-001	2.9	0.1	0.0	4.5	0.6	2.46	2.41	2.52	2.11	±	0.06	0.60	±	0.35	9668.60	±	4177.81	4.61	±	0.46	35184.67	0.58	0.46	0.43	0.13	0.59
JH-002	2.9	0.0	0.0	4.9	0.2	2.38	2.30	2.50	2.27	±	0.07	1.30	±	0.17	1010.37	±	257.67	2.56	±	0.10	17456.51	0.14	0.04	0.26	0.51	0.14
JH-005	0.0	2.9	0.0	5.1	0.0	2.02	2.02	2.02	2.06	±	0.05	10.33	±	2.08	90.73	±	14.88	0.00	±	0.00	1995.62	0.20	0.00	0.17	0.00	0.00
JH-007a	2.9	0.0	0.0	5.1	0.0	2.29	2.18	2.38	2.22	±	0.05	1.40	±	0.53	877.70	±	208.82	5.28	±	0.18	15825.40	0.38	0.04	0.24	0.27	0.38
JH-011	2.7	0.1	0.0	5.3	0.0	1.81	1.74	1.87	1.94	±	0.04	4.23	±	0.84	2815.70	±	884.70	0.97	±	0.35	4574.91	0.20	0.15	0.37	4.37	0.21
JH-013	2.9	0.0	0.0	4.9	0.1	2.63	2.58	2.65	2.49	±	0.08	0.85	±	0.21	666.10	±	164.63	25.70	±	0.52	29243.80	0.25	0.03	0.25	0.03	0.25
JH-016	2.8	0.1	0.0	5.0	0.1	2.49	2.45	2.53	2.40	±	0.06	0.97	±	0.15	613.07	±	137.12	0.85	±	0.07	24831.48	0.16	0.03	0.23	1.14	0.18
JH-017	0.3	2.6	0.0	5.0	0.1	2.29	2.26	2.34	2.11	±	0.05	3.97	±	0.23	2197.37	±	788.82	2.28	±	0.34	5316.19	0.06	0.10	0.36	1.74	0.16
JH-020	3.0	0.0	0.0	4.4	0.7	2.17	1.73	2.41	2.42	±	0.07	0.73	±	0.47	1112.70	±	331.76	13.28	±	0.21	32937.18	0.65	0.05	0.30	0.06	0.64
JH-022	0.6	2.4	0.0	4.8	0.2	2.34	2.27	2.34	2.27	±	0.05	4.53	±	0.29	207.93	±	25.85	0.41	±	0.00	5015.78	0.07	0.01	0.13	11.14	0.00
JH-025	2.6	0.3	0.0	4.6	0.5	2.47	2.42	2.52	2.47	±	0.07	1.07	±	0.23	385.17	±	72.33	6.31	±	0.27	23114.41	0.22	0.02	0.19	0.17	0.22
JH-028b	2.9	0.0	0.0	4.7	0.4	2.49	2.42	2.54	2.43	±	0.07	0.35	±	0.35	76.23	±	3.56	0.31	±	0.00	69370.86	1.01	0.00	0.05	1.14	0.00
JH-036	0.2	2.8	0.0	4.8	0.2	2.30	2.28	2.31	2.29	±	0.06	5.20	±	0.17	171.47	±	19.06	0.50	±	0.14	4410.15	0.04	0.01	0.11	10.36	0.29
JH-045	2.9	0.0	0.0	5.1	0.0	2.52	2.52	2.53	2.41	±	0.07	0.83	±	0.29	79.60	±	2.35	0.67	±	0.07	28887.12	0.35	0.00	0.04	1.25	0.36
JH-048	2.9	0.0	0.0	5.0	0.1	2.43	2.10	2.58	2.20	±	0.06	1.00	±	0.28	165.90	±	12.90	0.19	±	0.00	22005.67	0.28	0.01	0.08	5.26	0.00
JH-053	0.2	0.2	2.3	5.3	0.0	2.34	2.20	2.42	2.37	±	0.08	13.13	±	0.76	34.90	±	9.71	0.86	±	0.38	1802.53	0.07	0.00	0.28	15.31	0.44
JH-054	0.1	0.3	2.3	5.3	0.0	2.31	2.23	2.37	2.22	±	0.06	11.77	±	1.47	5926.77	±	2512.50	0.00	±	0.00	1883.60	0.13	0.27	0.42	0.00	0.00
JH-058	0.1	2.9	0.0	5.0	0.0	2.32	2.16	2.42	2.33	±	1.14	14.00	±	0.66	183.70	±	16.20	0.00	±	0.00	1664.24	0.74	0.01	0.74	0.00	0.00
JH-066	2.6	0.2	0.0	5.1	0.1	2.20	2.19	2.21	2.12	±	0.05	1.03	±	0.76	1250.23	±	379.91	0.46	±	0.00	20486.94	0.74	0.06	0.30	2.24	0.00
JH-074	2.3	0.5	0.0	5.2	0.0	2.49	2.46	2.51	2.16	±	0.06	2.33	±	0.55	36.17	±	4.44	3.20	±	0.21	9277.27	0.24	0.00	0.13	0.73	0.25
JH-076	0.5	2.5	0.0	5.1	0.0	2.34	2.24	2.46	2.03	±	0.05	12.43	±	0.76	51.80	±	8.52	0.00	±	0.00	1631.12	0.07	0.00	0.17	0.00	0.00
JH-077	0.0	3.0	0.0	5.1	0.0	2.32	2.28	2.36	2.16	±	0.07	20.23	±	1.45	52.30	±	9.75	0.00	±	0.00	1068.89	0.08	0.00	0.19	0.00	0.00

This is a preprint, the final version is subject to change, of the American Mineralogist (MSA)
Cite as Authors (Year) Title. American Mineralogist, in press.
DOI: https://doi.org/10.2138/am-2019-7068

JH-079	2.8	0.0	0.0	5.1	0.0	2.46	2.38	2.56	2.34	±	0.07	1.87	±	0.21	3151.43	±	1223.35	3.86	±	0.06	12541.52	0.12	0.13	0.39	0.48	0.11
JH-086	2.7	0.2	0.0	5.0	0.1	2.54	2.51	2.59	2.42	±	0.07	0.90	±	0.52	394.63	±	83.39	0.70	±	0.15	26930.56	0.58	0.02	0.21	1.28	0.61
JH-087	2.9	0.0	0.0	4.9	0.2	2.56	2.46	2.64	2.38	±	0.07	1.10	±	0.36	5851.77	±	2442.42	3.14	±	0.14	21617.00	0.33	0.25	0.42	0.35	0.33
JH-089	0.1	3.0	0.0	5.0	0.0	2.43	2.42	2.46	2.28	±	0.04	1.20	±	0.98	403.43	±	33.64	0.95	±	0.00	19040.89	0.82	0.02	0.09	1.26	0.00
JH-092a	2.8	0.0	0.0	5.0	0.2	2.49	2.43	2.57	2.40	±	0.07	1.17	±	0.23	59.53	±	2.41	0.61	±	0.03	20580.17	0.20	0.00	0.05	1.90	0.20
JH-094	2.8	0.0	0.0	5.1	0.0	2.54	2.46	2.59	2.34	±	0.09	1.03	±	0.21	366.13	±	47.74	2.40	±	0.43	22642.23	0.20	0.02	0.14	0.43	0.27
JH-097a	2.9	0.0	0.0	5.2	0.0	2.37	2.25	2.50	2.37	±	0.08	1.40	±	0.26	73.57	±	1.70	0.80	±	0.00	16910.79	0.19	0.00	0.04	1.76	0.19
JH-101	2.9	0.0	0.0	4.2	1.0	2.70	2.63	2.74	2.50	±	0.08	0.73	±	0.47	143.07	±	13.37	1.22	±	0.07	34088.59	0.65	0.01	0.10	0.60	0.65
JH-102	1.5	1.4	0.0	5.1	0.0	2.38	2.37	2.39	2.07	±	0.06	10.83	±	0.55	105.27	±	6.68	1.49	±	0.15	1915.05	0.06	0.01	0.07	7.28	0.12
JH-112	2.7	0.2	0.0	5.0	0.1	2.49	2.46	2.56	2.48	±	0.07	1.40	±	0.56	47.00	±	4.00	9.34	±	0.98	17709.93	0.40	0.00	0.09	0.15	0.41
JH-113	2.7	0.1	0.0	4.8	0.4	2.59	2.47	2.75	2.51	±	0.07	1.73	±	0.31	51.37	±	3.49	10.08	±	0.26	14453.56	0.18	0.00	0.07	0.17	0.18
JH-117	2.8	0.0	0.0	5.2	0.0	2.21	2.13	2.34	1.97	±	0.04	1.00	±	0.10	239.90	±	23.45	2.87	±	0.06	19745.40	0.05	0.01	0.12	0.35	0.05
JH-118	2.9	0.0	0.0	5.0	0.2	2.38	2.20	2.56	2.32	±	0.06	0.53	±	0.45	189.30	±	18.42	1.13	±	0.27	43513.31	0.85	0.01	0.10	0.47	0.88
JH-119	2.9	0.0	0.0	5.2	0.0	2.39	2.33	2.43	2.21	±	0.06	1.17	±	0.23	129.43	±	9.13	2.62	±	0.17	18937.26	0.20	0.01	0.08	0.44	0.21
JH-120									2.42	±	0.07	0.93	±	0.38	111.43	±	6.73	1.75	±	0.39	25933.61	0.41	0.00	0.07	0.53	0.46
JH-121	2.9	0.0	0.0	5.0	0.2	2.34	2.15	2.53	2.31	±	0.06	0.90	±	0.26	112.57	±	7.55	2.53	±	0.13	25709.33	0.30	0.00	0.07	0.36	0.30
JH-122	2.8	0.0	0.0	5.2	0.0	2.43	2.37	2.48	2.28	±	0.06	1.03	±	0.15	86.33	±	2.76	0.12	±	0.00	22087.39	0.15	0.00	0.04	8.33	0.00
JH-128e	0.3	2.7	0.0	4.6	0.5	2.38	2.33	2.42	2.34	±	0.06	4.37	±	0.21	133.27	±	9.87	0.00	±	0.00	5354.43	0.05	0.01	0.08	0.00	0.00
JH-129a	1.3	1.7	0.0	4.9	0.2	2.15	1.97	2.26	2.20	±	0.06	4.97	±	0.47	346.90	±	62.57	0.89	±	0.39	4422.26	0.10	0.02	0.18	5.58	0.44

This is a preprint, the final version is subject to change, of the American Mineralogist (MSA)
Cite as Authors (Year) Title. American Mineralogist, in press.
DOI: https://doi.org/10.2138/am-2019-7068

Sample	Mineral phase	# Ca	# P	#Pb	Cl (EPMA) wt%	F (SIMS) μg g^{-1}	Br (SIMS) μg g^{-1}	I (SIMS) μg g^{-1}	F (EPMA) μg g^{-1}
JH-078-01	pym	0.16	0.98	0.84	2.28	107.31	3.94	2.01	b.d.l.
JH-078-02	pym	0.14	0.98	0.86	2.31	50.71	3.65	1.76	b.d.l.
JH-078-03	pym	0.18	0.98	0.82	2.28	143.45	4.22	2.51	b.d.l.
JH-078-04	pym	0.25	0.98	0.75	1.92	175.60	4.83	1.29	b.d.l.
JH-078-05	pym	0.11	0.97	0.89	2.25	108.32	2.92	1.23	b.d.l.
JH-078-06	pym	0.04	0.92	0.96	2.21	22.99	3.79	0.65	b.d.l.
JH-078-07	pym	0.01	0.85	0.99	2.23	32.68	3.35	1.21	b.d.l.
JH-092b-01	pym	0.08	0.99	0.92	2.25	140.63	4.51	0.23	b.d.l.
JH-092b-02	pym	0.11	0.98	0.89	2.35	115.39	3.42	0.32	b.d.l.
JH-092b-03	pym	0.07	0.99	0.93	2.33	97.13	2.53	0.08	b.d.l.
JH-092b-04	pym	0.14	0.99	0.86	2.48	160.45	2.30	0.18	b.d.l.
JH-092b-05	pym	0.08	0.99	0.92	2.18	143.67	4.56	0.49	346.00
JH-092b-06	pym	0.15	0.99	0.85	2.30	214.86	4.94	1.14	b.d.l.
JH-096-01	pym	0.04	0.97	0.96	2.09	174.75	6.01	1.43	b.d.l.
JH-096-02	pym	0.15	0.98	0.85	2.18	202.60	4.18	1.41	b.d.l.
JH-096-03	pym	0.14	0.98	0.86	2.28	258.60	3.87	0.76	b.d.l.
JH-096-04	pym	0.23	0.99	0.77	2.30	408.51	4.01	1.01	b.d.l.
JH-096-05	pym	0.28	1.00	0.72	2.34	1407.06	9.08	0.50	b.d.l.
JH-096-06	pym	0.10	0.97	0.90	2.19	177.63	4.01	1.48	b.d.l.
JH-114-01a	mim	0.17	0.13	0.83	2.21	791.61	6.84	0.08	104.00
JH-114-01b	mim	0.16	0.14	0.84	2.18	968.03	6.76	0.08	204.00
JH-114-02a	mim	0.05	0.14	0.95	2.13	55.90	6.64	0.07	b.d.l.
JH-114-02b	mim	0.03	0.10	0.97	2.07	128.01	7.52	0.09	b.d.l.
JH-114-03	mim	0.01	0.09	0.99	2.01	46.91	15.03	0.26	116.00
JH-114-04	mim	0.05	0.03	0.95	2.17	73.94	12.82	0.15	b.d.l.
JH-114-05	mim	0.01	0.34	0.99	2.06	2857.82	3.75	2.41	208.00
JH-114-06	mim	0.12	0.91	0.88	2.24	1216.88	1.83	1.43	b.d.l.
JH-117-01	pym	0.00	0.99	1.00	2.07	78.83	2.11	3.00	442.00
JH-117-02	pym	0.00	0.99	1.00	1.98	141.10	1.30	3.77	b.d.l.
JH-117-03	pym	0.00	0.97	1.00	2.01	178.74	3.47	2.96	b.d.l.
JH-118-01	pym	0.00	1.00	1.00	1.97	400.19	2.27	2.04	b.d.l.
JH-118-02	pym	0.05	0.99	0.95	2.21	313.08	2.42	1.09	248.00
JH-118-03	pym	0.05	0.99	0.95	2.05	385.41	2.03	1.96	b.d.l.
JH-118-04	pym	0.04	0.99	0.96	2.04	339.22	2.95	2.94	b.d.l.
JH-118-05	pym	0.02	0.99	0.98	2.09	191.32	1.64	2.51	b.d.l.
JH-118-06	pym	0.00	1.00	1.00	2.26	17.55	0.61	0.08	95.00
JH-119-01	pym	0.00	1.00	1.00	2.06	33.47	0.86	1.52	b.d.l.
JH-119-02	pym	0.00	1.00	1.00	2.02	43.62	1.02	2.53	b.d.l.
JH-122b-L01	pym	0.00	1.00	1.00	2.10	79.28	2.79	0.96	b.d.l.
JH-122b-L02	pym	0.00	1.00	1.00	2.03	141.06	3.62	1.36	b.d.l.
JH-122b-L03	pym	0.00	1.00	1.00	2.14	39.48	0.72	1.31	b.d.l.
JH-122b-L04	pym	0.00	1.00	1.00	2.16	81.01	1.65	3.60	b.d.l.
JH-122b-L05	pym	0.00	1.00	1.00	2.12	31.98	0.76	1.13	b.d.l.
JH-122b-L06	pym	0.00	1.00	1.00	2.15	33.59	0.89	1.49	b.d.l.
JH-122b-L07	pym	0.00	1.00	1.00	2.17	36.85	0.78	1.00	b.d.l.
JH-122b-L08	pym	0.00	0.98	1.00	2.16	59.45	1.77	0.70	172.00
JH-122b-L09	pym	0.01	1.00	0.99	2.12	63.75	1.67	0.39	b.d.l.
JH-122b-	pym	0.00	1.00	1.00	2.11	56.21	0.91	0.76	b.d.l.

This is a preprint, the final version is subject to change, of the American Mineralogist (MSA)
Cite as Authors (Year) Title. American Mineralogist, in press.
DOI: https://doi.org/10.2138/am-2019-7068

Q01									
JH-122b-Q02c	pym	0.00	1.00	1.00	2.17	38.75	0.59	0.41	138.00
JH-122b-Q03	pym	0.00	1.00	1.00	2.11	83.32	1.37	1.41	b.d.l.
JH-122b-Q04	pym	0.00	1.00	1.00	2.16	101.92	1.45	1.55	b.d.l.
JH-122b-Q05	pym	0.00	0.99	1.00	2.07	42.58	0.73	0.58	b.d.l.
JH-122b-Q06	pym	0.00	1.00	1.00	2.21	49.07	0.85	0.65	b.d.l.
JH-122b-Q07	pym	0.00	1.00	1.00	2.16	39.62	0.74	1.01	b.d.l.
JH-122b-Q08	pym	0.00	0.99	1.00	2.05	176.41	2.46	1.39	b.d.l.
JH-127a-01	pym	0.01	0.99	0.99	2.16	100.28	1.51	12.88	b.d.l.
JH-127a-02	p.hed	0.21	1.00	0.79	2.13	2023.25	1.39	27.38	b.d.l.
JH-127a-04	p.hed	0.25	0.99	0.75	2.03	2211.58	1.25	21.62	790.00
JH-127a-05	p.hed	0.21	1.00	0.79	2.17	1811.16	1.46	26.13	242.00
JH-127a-06	p.hed	0.25	0.99	0.75	2.12	2604.03	1.26	24.47	b.d.l.
JH-127a-08	p.hed	0.23	1.00	0.77	2.23	1651.89	1.24	30.93	b.d.l.
JH-128b-01	mim	0.12	0.13	0.88	2.09	341.55	7.32	0.05	705.00
JH-128b-02	mim	0.12	0.11	0.88	2.15	559.65	7.82	0.05	983.00
JH-128b-03	mim	0.13	0.11	0.87	2.14	390.17	6.59	0.06	b.d.l.
JH-128b-04	mim	0.11	0.11	0.89	2.17	334.26	7.62	0.04	b.d.l.
JH-128b-05	mim	0.00	0.10	0.88	2.13	695.73	7.25	0.04	b.d.l.
JH-128b-06	mim	0.15	0.10	0.85	2.12	1057.03	7.28	0.04	195.00
JH-129b-01	P-mim	0.11	0.61	0.89	1.82	3698.53	11.89	2.46	1034.00
JH-129b-02	P-mim	0.09	0.55	0.91	2.15	475.38	10.61	1.76	b.d.l.
JH-129b-03	P-mim	0.04	0.45	0.96	2.09	168.56	10.28	0.87	311.00
JH-129b-04	P-mim	0.05	0.50	0.95	2.08	222.37	7.97	0.86	b.d.l.
JH-129b-05	P-mim	0.07	0.48	0.93	2.06	286.06	12.53	1.15	574.00
JH-129b-06	P-mim	0.09	0.54	0.91	2.10	532.83	10.34	1.86	b.d.l.
JH-129b-07	p.hed	0.39	0.98	0.61	0.06	98643.37	39.38	31.07	12700.00
JH-129b-08	P-mim	0.06	0.60	0.94	2.20	291.26	15.75	0.27	b.d.l.

Sample type		Region	Absolute concentration (mg kg^{-1},L^{-1})				Reference
			Cl	F	Br	I	
Water	Rain water	Tübingen; DE	0.121	0.0121	b.d.l.		Göb et al. (2013)
	Rain water	Hafren forest, UK	4.49		0.0172	0.013	Neal et al. (2010)
	Rain water	New Hampshire, USA	4.35-8.16				Lovett et al. (1996)
	Rain water	Chile	0.5		0.0039	0.00048	Biester et al. (2006)
	Cloud water	Hafren forest, UK	47.8		0.156	0.00848	Neal et al. (2010)
	Throughfall	Slavkov forest; CZ	0.029-0.041				Krám et al. (1997)
	Throughfall (under sugar maple)	Hardwood forest, USA	1.29-2.35				Eaton et al. (1973)
	Throughfall (under yellow birch)	Hardwood forest, USA	0.93-0.95				Eaton et al. (1973)
	Throughfall (under beech)	Hardwood forest, USA	0.75-1.25				Eaton et al. (1973)
	Creek water	Feldberg; DE	0.393	0.0233	b.d.l.		Göb et al. (2013)
	Creek water	Oberwolfach; DE	1.44	0.58	0.00675		Göb et al. (2013)
	Stream water	Slavkov forest, CZ	0.069-0.0665				Krám et al. (1997)
	Mine water	Feldberg; DE	0.744	0.0488	0.00454		Göb et al. (2013)
	Thermal water	Leuze, Stuttgart; DE	1070	1.21	1.96		Göb et al. (2013)
	Sea water		18800	1.3	67	0.06	(Wong and Brewer 1974; Wilson 1975; Whitfield and Turner 1979; Fuge 1988; Li 1991)
Soil	Agricultural soils	France	19-100 (med.:50)				Redon et al. (2013)
	Grassland soils	France	13-1248 (med.:54)				Redon et al. (2013)
	Forest soils	France	34-340 (med.:90)				Redon et al. (2013)
	Forest soils	Japan			68-130	20-23	Yuita et al. (1978)
	Humus layer forest soils	Norway	300-1200		5-100	3-20	Låg and Steinnes (1976)
	Organic rich soil – peat bog	Chile	350-1200		40-200	10-20	Biester et. al. (2004, 2006)
	A horizon soil forest	Tsukuba, Japan				70	Yuita et al. (2006)
	B horizon soil forest	Tsukuba, Japan				40-55	Yuita et al. (2006)

Rock leachates	Gneiss leachates	Schwarzwald, DE	0.1-2.4	0.002-0.75	b.d.l.-0.035		Burisch et al. (2016)
	Granite, leachates	Schwarzwald, DE	0.29-13.8	0.016-1.78	b.d.l.-0.144		Burisch et al. (2016)
	Sandstone, leachates	Schwarzwald, DE	0.12-2.68	0.012-0.027	b.d.l.-0.035		Burisch et al. (2016)
Rock	A-type granite	USA, Canada	45-400	400-12200			Eby (1990)
	Granite	Germany	70-300		<1-9.5		Behne (1953)
	Granite	Schwarzwald, DE	240	980	1.5		Burisch et al. (2016)
	Gabbro	Harzburg, DE	20		<1		Behne (1953)
	Basalt	Göttingen, DE	30-120		<1-2.2		Behne (1953)
	Keuper clay	Friedland a.d. Leine, DE	370		4.4		Behne (1953)
	Gneiss		140-1000		0.007-0.055		Johns and Huang (1967); Muramatsu and Wedepohl (1998)
	Gneiss	Schwarzwald, DE	120	600	0.4		Burisch et al. (2016)
	Amphibolites	China,	100-400	659	0.020-0.026		Johns and Huang (1967); Gao et al. (1998); Muramatsu and Wedepohl (1998)
	Sandstone	China	68-180	482-489			Gao et al. (1998)
	Sandstone	Schwarzwald, DE	47	68	0.5		Burisch et al. (2016)
Vegetation	Wood	New Hampshire, USA	9-185				Lovett et al. (2005)
	Bark	New Hampshire, USA	37-170				Lovett et al. (2005)
	Foliage (temperate-zone forest)	New Hampshire, USA	9-2500				Lovett et al. (2005)

This is a preprint, the final version is subject to change, of the American Mineralogist (MSA)
Cite as Authors (Year) Title. American Mineralogist, in press.
DOI: https://doi.org/10.2138/am-2019-7068

Fig. 1

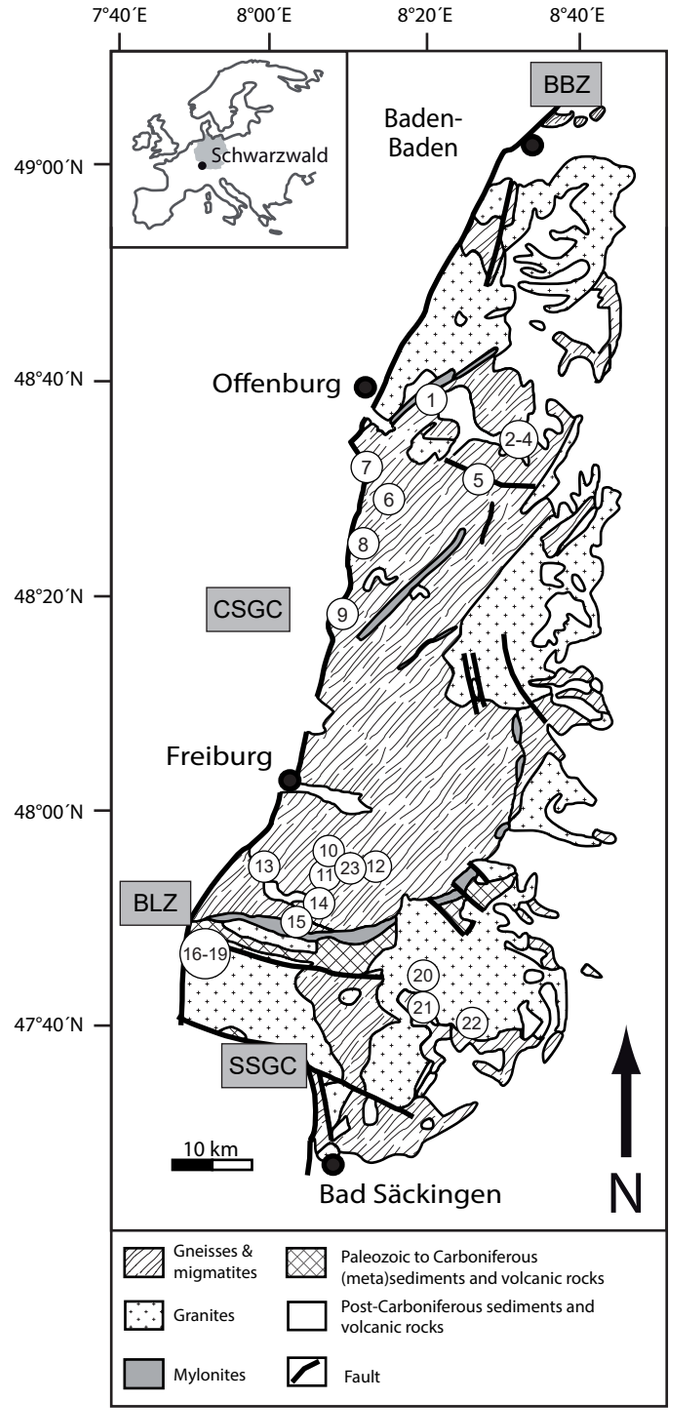

This is a preprint, the final version is subject to change, of the American Mineralogist (MSA)
Cite as Authors (Year) Title. American Mineralogist, in press.
DOI: https://doi.org/10.2138/am-2019-7068

Fig. 2

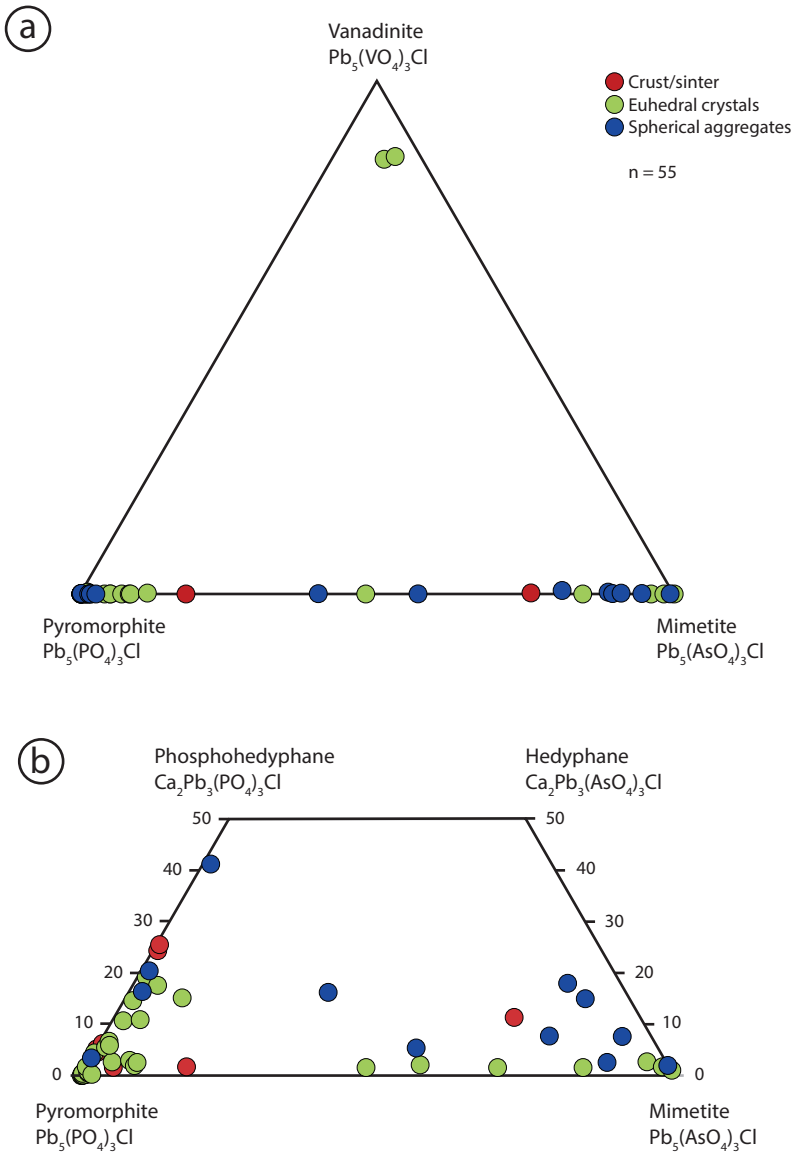

This is a preprint, the final version is subject to change, of the American Mineralogist (MSA)
Cite as Authors (Year) Title. American Mineralogist, in press.
DOI: https://doi.org/10.2138/am-2019-7068

Fig. 3

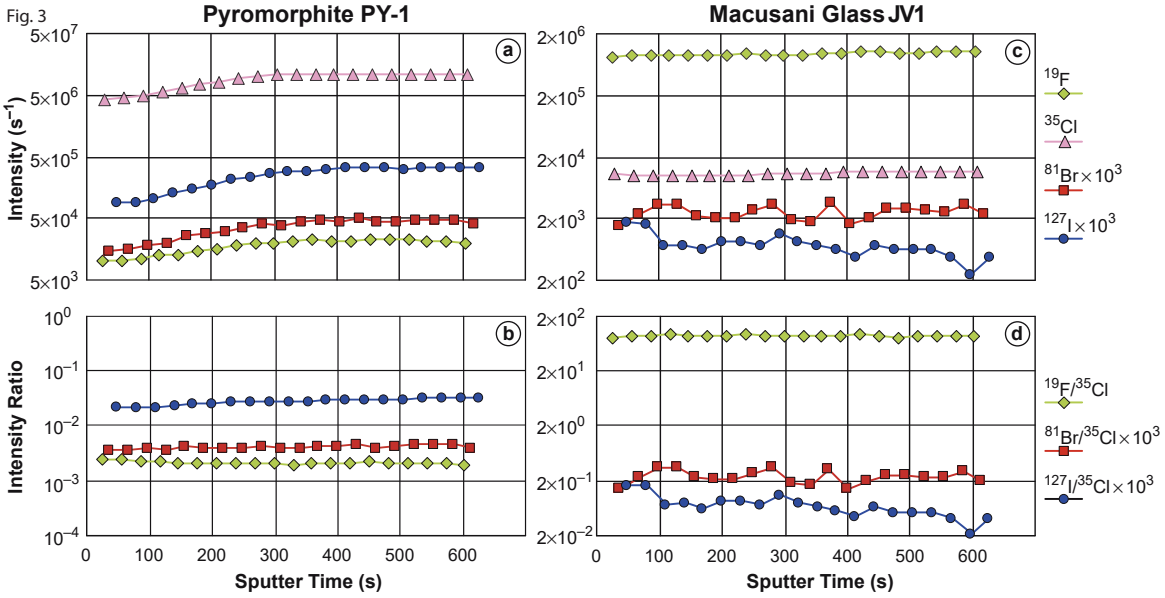

This is a preprint, the final version is subject to change, of the American Mineralogist (MSA)
Cite as Authors (Year) Title. American Mineralogist, in press.
DOI: https://doi.org/10.2138/am-2019-7068

Fig. 4

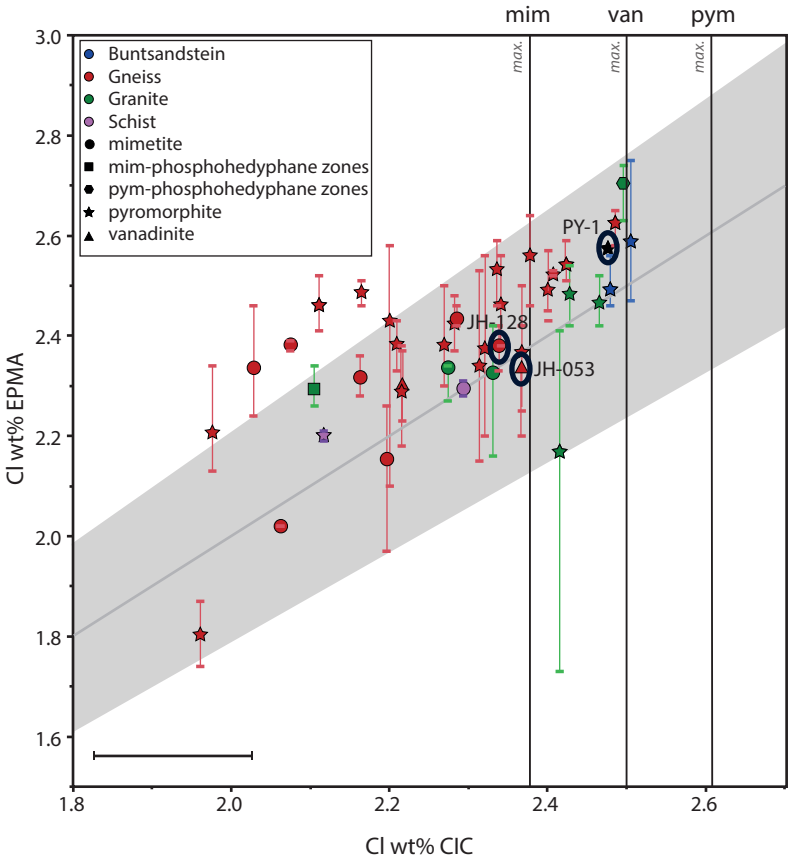

This is a preprint, the final version is subject to change, of the American Mineralogist (MSA)
Cite as Authors (Year) Title. American Mineralogist, in press.
DOI: https://doi.org/10.2138/am-2019-7068

Fig. 5

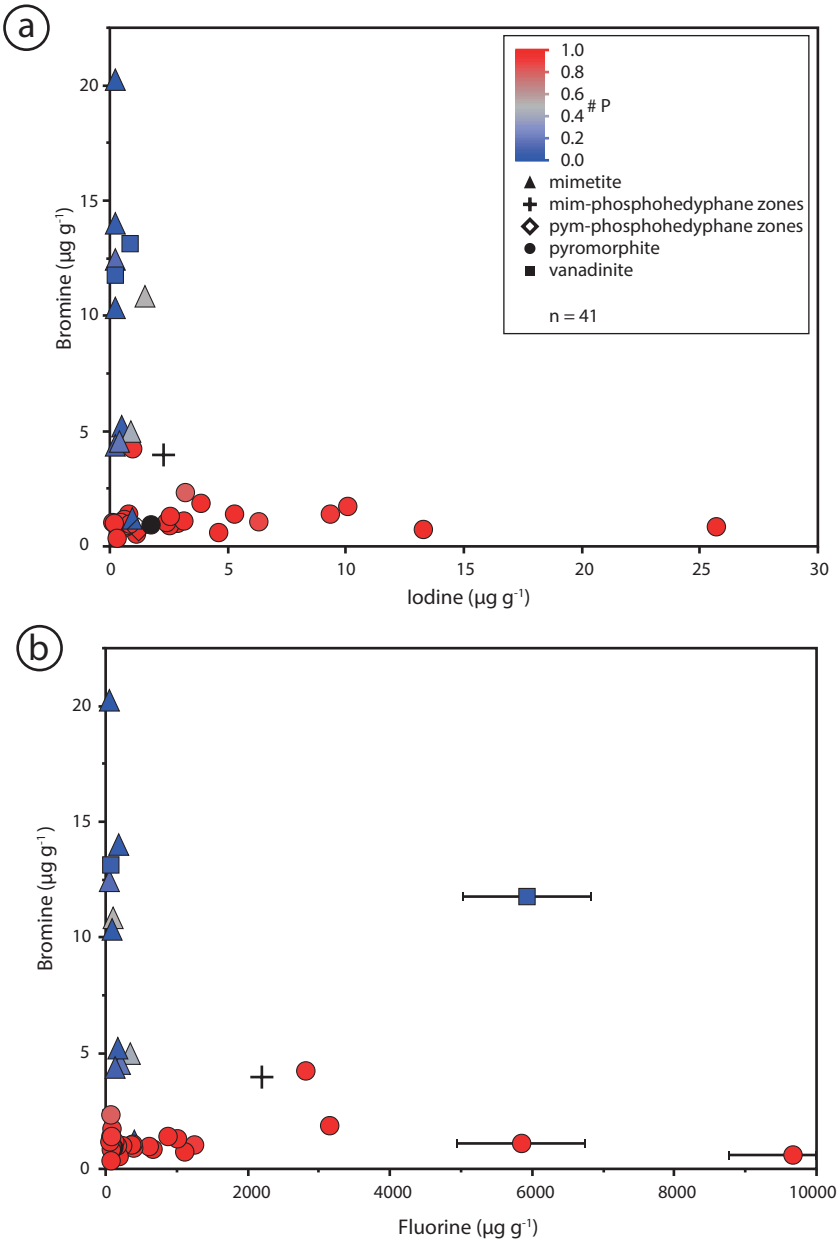

This is a preprint, the final version is subject to change, of the American Mineralogist (MSA)
Cite as Authors (Year) Title. American Mineralogist, in press.
DOI: https://doi.org/10.2138/am-2019-7068

Fig. 6

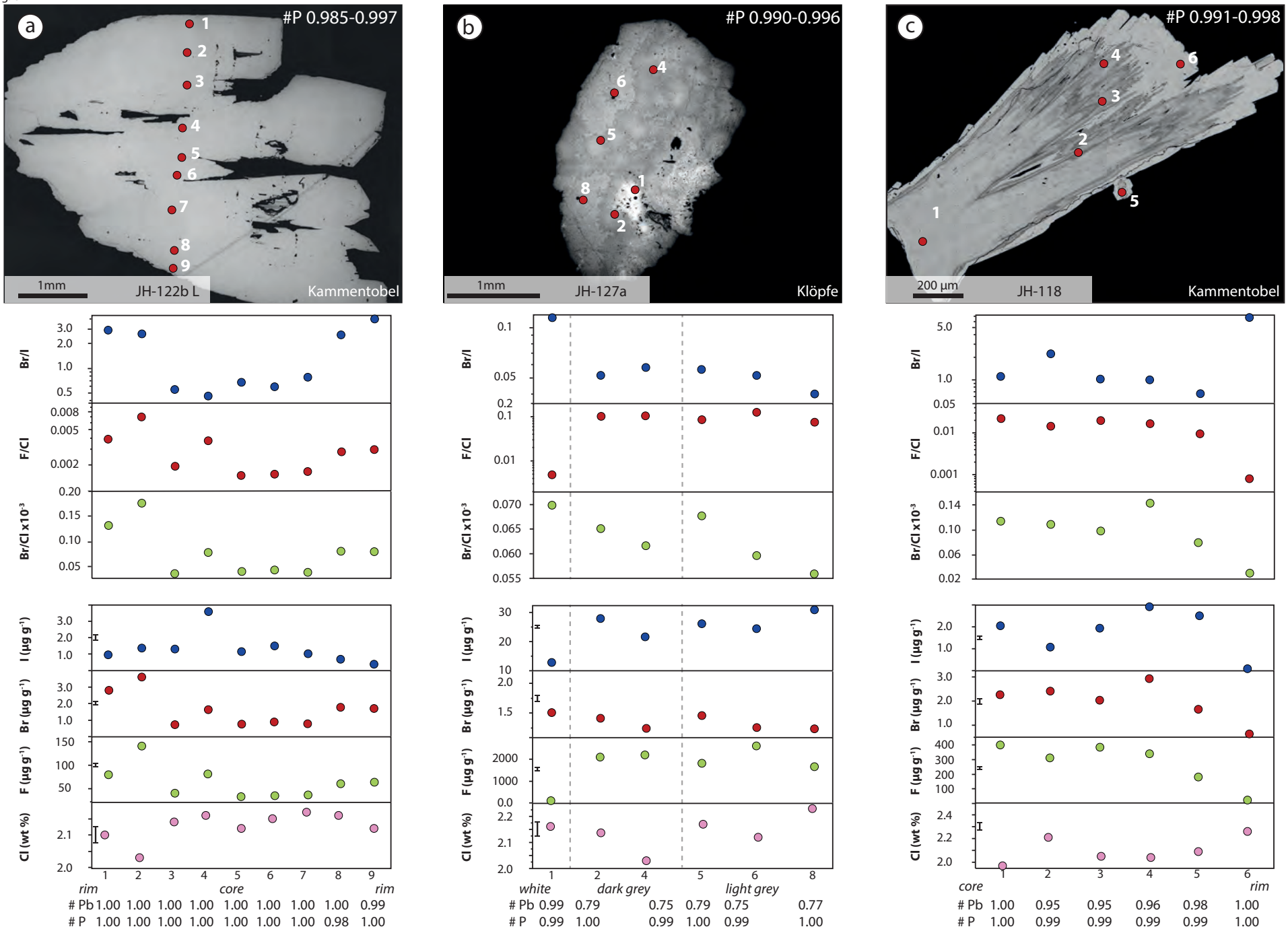

This is a preprint, the final version is subject to change, of the American Mineralogist (MSA)
Cite as Authors (Year) Title. American Mineralogist, in press.
DOI: https://doi.org/10.2138/am-2019-7068

Fig. 7

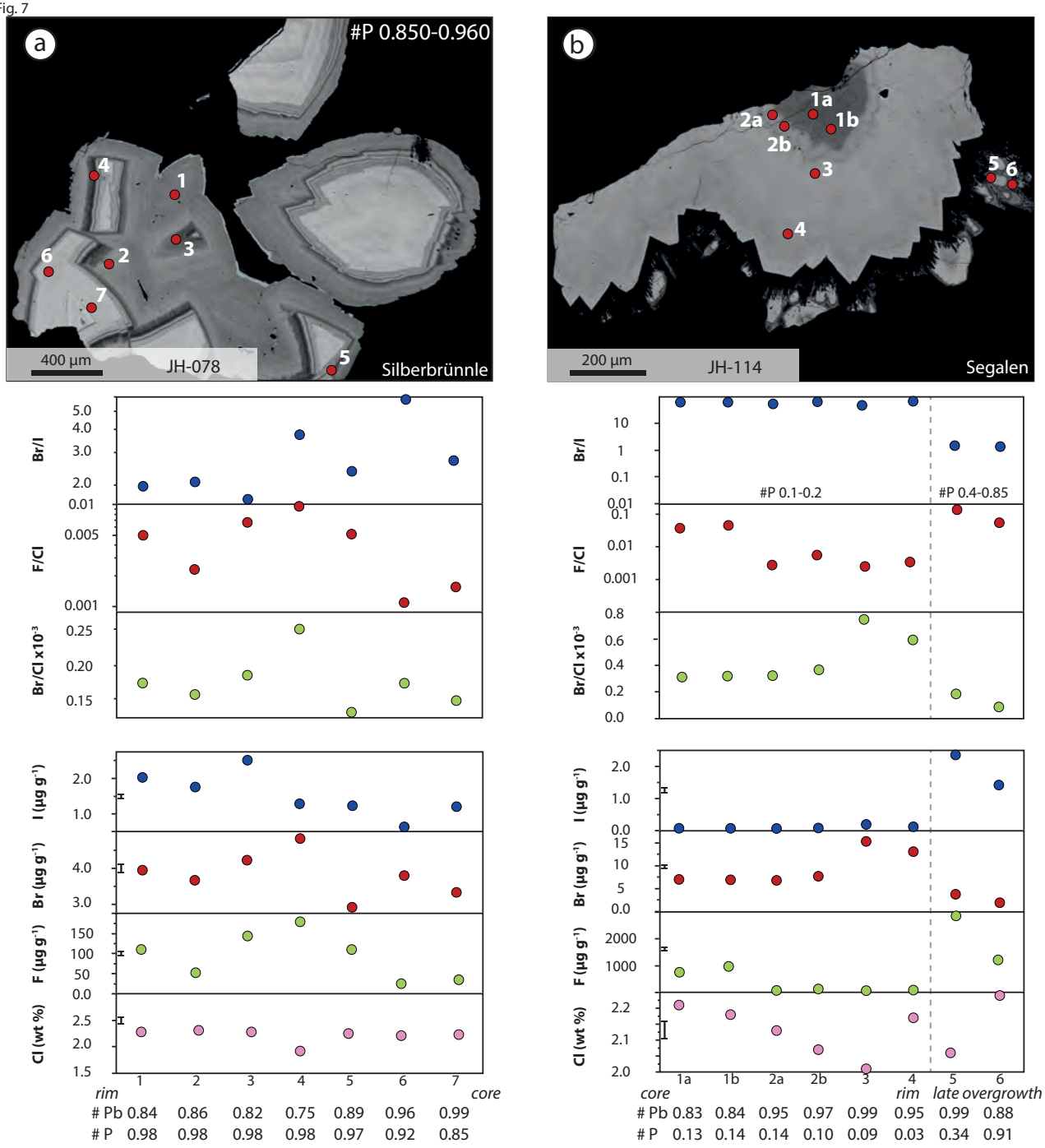

This is a preprint, the final version is subject to change, of the American Mineralogist (MSA)
Cite as Authors (Year) Title. American Mineralogist, in press.
DOI: https://doi.org/10.2138/am-2019-7068

Fig. 8

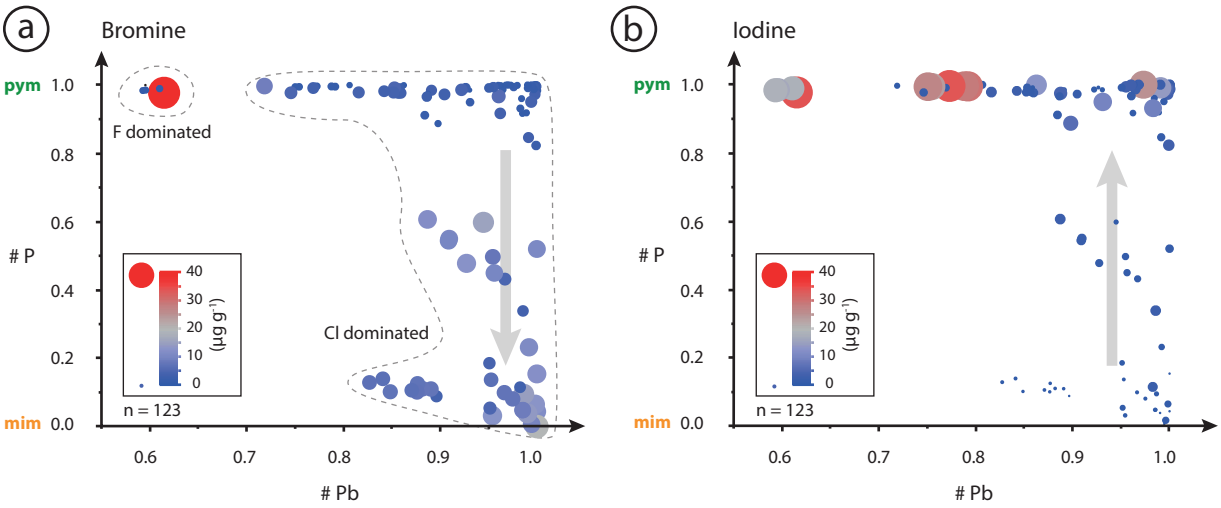

This is a preprint, the final version is subject to change, of the American Mineralogist (MSA)
Cite as Authors (Year) Title. American Mineralogist, in press.
DOI: https://doi.org/10.2138/am-2019-7068

Fig. 9